8-2019

Numerical Simulation of Diffuse Ultrasonic Waves in Concrete

Hossein Ariannejad
University of Nebraska - Lincoln, h.a.nejad19@gmail.com

NUMERICAL SIMULATION OF DIFFUSE ULTRASONIC WAVES IN CONCRETE

by

Hossein Ariannejad

A THESIS

Presented to the Faculty of
The Graduate College at the University of Nebraska
In Partial Fulfillment of Requirements
For the Degree of Master of Science

Major: Civil Engineering

Under the supervision of Professor Jinying Zhu

Lincoln, Nebraska

August, 2019

NUMERICAL SIMULATION OF DIFFUSE ULTRASONIC WAVES IN CONCRETE

Hossein Ariannejad, M.S
University of Nebraska, 2019

Advisor: Jinying Zhu

Concrete can be subject to various type of damages. Some damages such as Alkali Silica Reaction (ASR) tend to start from the inside, where there is no easy way to identify or evaluate them in the early stage. The study of ultrasonic waves scatterings in non destructive testing (NDT) methods play a major role in identifying such damages.

In an ultrasonic test, high frequency ultrasonic waves are used to interrogate the internal structure of concrete material, where the coarse aggregates and microcracks cause multiple scattering of ultrasonic waves. Experimental studies have demonstrated that diffuse ultrasonic waves scattered by boundaries, coarse aggregates, and microcracks are very sensitive to microstructural change in concrete. There are extensive studies implementing various experimental ultrasonic methods to detect and monitor the small changes within the concrete structure. However, there are not many numerical simulations of wave propagation in concrete to study the effects of such small changes in concrete in the receiving signals.

In this Thesis, a numerical method to model concretes with microcracks in different damage stages is proposed. First, a finite element model of a concrete sample that includes mortar and a random set of aggregates is simulated. For each damage stage,

a series of randomly sized and oriented cracks that are partially filled with the ASR gel is added to the sample. Each damage stage can be quantified based on the number of cracks in a normalized surface area. At each stage, an elastic wave is sent through the sample, and a series of Coda Wave Interferometry (CWI) and ultrasound diffusion approximation is then used to compare the velocity change, diffusivity, and dissipation of the receiving signals. Results suggest there is a direct relationship between the damage stages and the mentioned ultrasonic wave factors. The proposed method can be used for nondestructive evaluation and quantification of the damage such as ASR in concrete structures.

Acknowledgements

First and foremost, I would like to express my sincerest gratitude to my advisor Professor Jinying Zhu. She was not only a great advisor but also an outstanding teacher, mentor, and role play. The door to Professor Zhu's office was always open whenever I had a question or concern regarding my research, and she was always ready to help me with her insightful comments and advice. I could not have imagined having a better advisor and mentor for my study.

I would also like to thank Prof. Joshua Steelman and Prof. Seunghee Kim for accepting to be part of my thesis committee.

I am grateful to all of those with whom I have had the pleasure to work with at the University of Nebraska-Lincoln Non-Destructive Testing lab for providing a nice working environment.

Furthermore, the financial support provided by the Department of Energy is greatly appreciated.

Finally, I would like to express my loving gratitude to my dear family for their endless support and encouragement. Their unconditional love and support are always the biggest motivations behind all my achievements.

Contents

List of Figures

CHAPTER 1

Introduction

Concrete is the most widely used construction material in the world, and like any other materials, it is subject to various forms of physical and chemical damages. Detecting damages at early stages can be helpful to reduce the repair cost and increase the structure durability.

Nondestructive testing (NDT) methods can provide an evaluation of the concrete quality without causing any damages. Many NDT methods used in concrete structure inspections such as Ultrasonic Pulse Velocity (UPV) [2], Impact-Echo (IE) [3] are based on ultrasonic wave propagation. The UPV method is based on measuring the first arrival time of the pulse sent by the transducer. The IE uses a low frequency impact that propagates inside the concrete and the reflection by the damages or boundaries is recorded by a receiver. The main disadvantage of conventional NDT methods such as UPV or impact-echo is that the time of the first arrival and the low frequency waves employed in these methods are not sensitive to small damages. Therefore, they are not ideal for detecting such damages at very early stages. In order to detect microcracks, the wavelength of the ultrasonic wave should be smaller than or in the same order of the cracks. Such wavelengths in concrete correspond to frequencies well above 100 kHz. Utilizing waves with such high frequencies in a heterogenous material like concrete results in large scattering by the aggregates and cracks and high attenuation of the

wave energy.

Recently various NDT methods have been introduced to detect the microcrack damages using the diffuse wave field. Wave diffusion analysis is one of the recent methods based on utilizing high frequency diffuse wave. Experimental studies have demonstrated that diffuse ultrasonic waves scattered by boundaries, coarse aggregates, and microcracks are very sensitive to microstructural change in concrete. Anugonda et al. [4] demonstrated the ultrasonic energy density in concrete follows the diffusion equation and is a function of diffusivity (D) and dissipation (σ) parameters. By increasing the ultrasonic frequency the dissipation would increase and the diffusion decreases. They suggested in case of distribution of microcracks in the material the measured diffusion value would decrease. Ramamoorthy et al. [5] used ultrasound diffusion to determine the crack depth. They demonstrated that ultrasonic wave filed in a concrete slab can be modeled as a two-dimensional diffusion process. The arrival time of the peak diffuse energy at the receiver get delayed by the presence of a crack. They showed this delay increases considerably with the increase in crack depth. Deroo et al. [6, 7] employed the diffusion method to study the relation between Alkali Silica Reaction (ASR) and thermal damage with the diffusivity and dissipation factors. They suggested for both cases there is a clear trend between the damage level and the diffusivity factor. They showed that with increase of the damage level the diffusivity decreases. Meanwhile, the dissipation stays almost the same for the ASR damage and with regard to the thermal damage, and it does not follow a certain pattern with regard to the damage level.

Another analysis method utilizing the high frequency diffuse wave is the coda wave interferometry (CWI). Signals passed through a heterogeneous material like concrete can be separated into two parts. The first part is the coherent wave that travels a direct path from the source. The tail part that comes later and is diffused by the scatterers is called the coda wave. Since the coda part of a signal has a longer travel path due to

the scattering by the heterogeneities, it is more sensitive to small changes inside the material than the coherent part. The CWI analysis is based on comparing the coda of signals before and after a weak change in material. This relative velocity change between the coda parts of the two signals can be used as a representation of the change inside the medium. Snieder et. al [8] first introduced the CWI analysis to study the

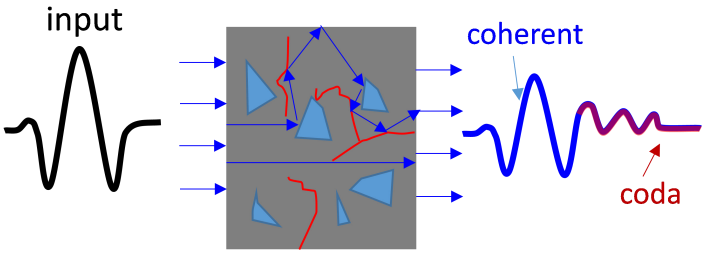

Figure 1.1: Multi-scattering of ultrasonic waves in concrete.

relation between the temperature change and the relative velocity change in granite. Lobkis and Weaver [9] introduced a new signal processing method for calculating the relative velocity change in a CWI analysis named Stretching technique. Comparing to the former method (doublet method) introduced by Sneider, the stretching technique uses a large portion of the signal to calculate the velocity change. With CWI analysis, Lacrose and Hall [10] found that a relative wave velocity change (dV/V) at a level of 10^{-5} can be reliably measured in concrete. Schurr et al. [11] demonstrated the CWI's ability to detect the damages caused by cyclic load and thermal damage.

The major challenge in the existing researches is that due to the experimental nature of these studies a quantitative relationship between the velocity change dV/V and microcracking damage level is not available.

Given the complex nature of the wave attenuation in concrete due to the existence of various heterogeneities with different shapes and sizes, there are very few studies of numerical simulations of the diffusive ultrasonic waves in concrete. Asadollahi and Khazanovich carried out a numerical simulation of shear wave attenuation in a 3D concrete model [12] and investigated the effect of shape, size, and material properties

of the aggregates on shear wave attenuation in concrete. They suggested that the maximum aggregate size and the material properties of aggregates have a significant role in the attenuation. On the other hand, the aggregate shape has a minimal effect on the shear wave attenuation.

The objective of this research task is to understand the scattering effects of coarse aggregates and microcracks on ultrasonic waves and develop a quantitative relationship between wave velocity change and mircocracking damage. This thesis presents a numerical simulation of elastic wave propagation in concrete - a complex, inhomogeneous medium with coarse aggregates and microcracks.

Chapter 2 first describes the procedure to build finite element models (FEM) with randomly distributed coarse aggregates of various shapes. Then models with random cracks are created. These two models are then combined to form a concrete model with randomly distributed aggregates and microcracks.

Chapter 3 presents wave propagation results using the models developed in chapter 2. The diffusion analysis method and the coda wave interferometry method are used to study the effects of aggregate shape and content, crack density and the input force frequency on the received signals from the concrete model simulations. One example of microcrack damage is caused by the ASR. Like most of the concrete deterioration mechanisms, ASR damage manifests as microcracks at early stages. ASR is a chemical reaction that forms an expansive gel inside aggregates and eventually causes a network of cracks inside the concrete, which can significantly decrease the strength and durability of concrete. Due to the importance and the prevalence of ASR damage in concrete structures, in this chapter, the effect of the ASR gel product inside cracks is also investigated.

Conclusions and future research suggestions are given in chapter 4.

In appendix A a detailed procedure of the aggregate generating algorithm and sample source codes are demonstrated.

Appendix B presents more details on importing the aggregate and cracks geometries from the MATLAB source code. It also shows the sample procedure of how the concrete model is generated in the ABAQUS program.

CHAPTER 2

Numerical Modeling of Wave Propagation in Concrete

2.1 Ultrasonic wave propagation in concrete

Conventional ultrasonic wave NDT methods measure signal travel times and amplitudes (coherent part only) in the material, and then use ultrasonic velocity and attenuation to estimate quality of concrete. To avoid strong scattering in a highly inhomogeneous and scattering medium like concrete, the ultrasonic wavelength (λ) should be larger than the aggregate ($\sim$ 25 mm). Therefore, most conventional ultrasonic methods for concrete NDT use low frequency ultrasounds (<100 kHz), and the common commercial transducers have a resonance frequency of 54 kHz. However, low frequency ultrasound cannot accurately characterize concrete degradation at early stages since the wavelengths are much larger than microcracks in concrete.

When the wavelengths of ultrasonic waves are smaller than or comparable to the size of scatters (aggregates, cracks), the waves will be scattered multiple times and take a long path before received by sensors, while the amplitude of coherent part of signal is attenuated. Because the scattering paths are random, the received signal has elongated duration and a noisy tail (coda wave). The diffuse ultrasonic signal contains

rich information about the medium because of multiple interactions between scattered waves and scatters (e.g. cracks). Therefore, diffuse wave is highly sensitive to small changes in the material such as microcracking initiation and development. Detailed analysis of diffuse waves will be presented in Chapter 3.

The typical frequency range used for diffuse ultrasonic wave test is $50 \sim 200$ kHz. Ultrasonic wave above 200 kHz will have high attenuation and very small penetration depth in concrete. In this frequency range, coarse aggregates and microcracks cause multi-scattering of ultrasonic waves, while the mortar matrix can be regarded as a homogeneous medium because the sizes of fine aggregates are much smaller than the wavelength. Therefore, in this study concrete is modelled as a homogeneous mortar matrix with randomly distributed aggregates and cracks. The following sections will present the procedures to simulate coarse aggregates of different shapes and microcracks.

2.2 Modeling of aggregates

2.2.1 Aggregate size distribution

Aggregate gradation is the size distribution of aggregate particles used in a concrete mixture and is determined by the passing percentage of the particles from multiple sieves of different sizes. Gradation can play a crucial role in concrete characteristics such as strength, durability, permeability, workability, shrinkage and creep. This distribution can be different based on the primary use of the desired concrete mixture. For instance, if all the aggregates were from the same size, concrete would have higher permeability and lower aggregate content, but if a concrete contains aggregate from a broader range of sizes, it can achieve a higher aggregate content. In normal con-

cretes, aggregates usually occupy 60-70 percent of the concrete volume. Fuller's curve is widely used to describe a maximum density gradation, as shown in the following formula:

$$P_i = (d_i/d_{max})^n \tag{2.1}$$

where the d_i represents the opening size of the i^{th} sieve, d_{max} the maximum particle size and P_i is the percentage passing the i^{th} sieve. The parameter n adjusts the fineness or coarseness, and when n=0.45, the gradation gives the highest density.

Based on Fuller's curve figure 2.1, for mixture with a maximum aggregate size of 19.5 mm, about 40 $\sim$ 50 percents of aggregates are larger than 5 mm. To reduce the model complexity only aggregates with diameters larger than 5 mm were generated. Smaller aggregates can be regarded as a portion of homogeneous mortar matrix. For a concrete model with total aggregate volume of 70%, the volumetric aggregate content in the size range of 5 mm-25 mm is about 28 $\sim$ 35 percent. In our simulation, we used about 35% aggregate content into the concrete model.

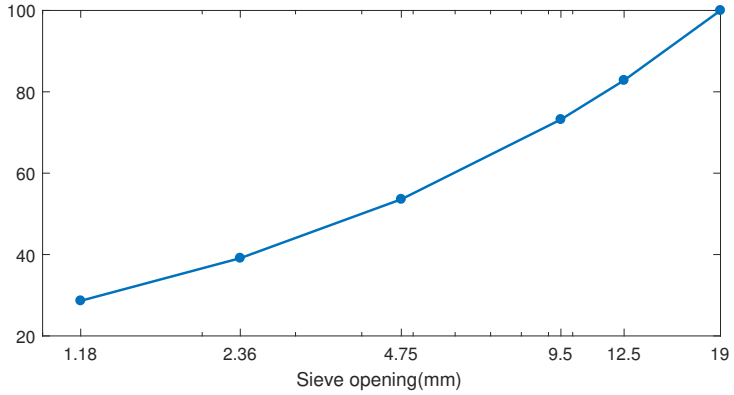

Figure 2.1: Fuller's ideal aggregate-size distribution curve

2.2.2 Circle-shaped aggregates

In order to generate circle-shaped aggregates, two sets of variables - the circle's center coordinates and radius, should be determined. The circle radius will be determined

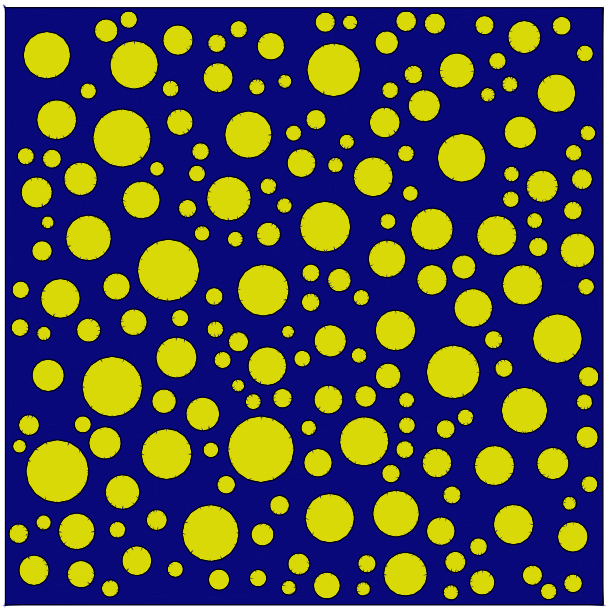

Figure 2.2: Randomly distributed circle-shaped aggregates placed in a 15 cm×15 cm model. Volume percentage of aggregates is about 35%.

based on aggregate size distribution from Fuller's curve (figure 2.1), and the center coordinates are two random numbers within the concrete model region. We assume no two aggregates have contact or overlap with each other. When the program generates the first aggregate, it checks if any point on the circle perimeter will be out of the sample borders. If so, it tries a new random position and will do that until the condition is satisfied. The next aggregate will be generated with the same procedure. However, this time there is an extra check to make sure the new aggregate has no conflict with existing ones, and in case there are any conflicts, the program tries new coordinates to place the aggregate. This condition can be checked by comparing the distance between two circles' centers and the sum of their radiuses $r_1 + r_2$. If the center distance between two circles is larger than $r_1 + r_2$, it means there is no conflict between two circles; otherwise, we have to change the placement of the new circle. Since larger aggregates play a more crucial role in wave reflection or attenuation, the aggregate placement algorithm starts with the larger aggregates first and gradually goes for the smaller ones. This procedure will continue until the sample reaches the desired aggregate volume percentage or after a large number of trials, it cannot find a

new position for the new aggregates.

2.2.3 Square-shaped aggregates

Generation of square-shaped aggregates follows a similar procedure as for the circle-shaped aggregates. However, overlap detection for squares is more complex than for the circle shapes. We decide to use a pixel method to check the aggregate conflict with the borders or with other aggregates. The pixel method treats the concrete cross section as a binary pixel image. For example, an 1 m $\times$ 1 m concrete section can be modeled as an image with 1000 $\times$ 1000 pixels, and each pixel represents an area of 1 mm^2. In the matrix of binary pixels, value 1 represents aggregate, and value 0 represents mortar. Before placing any aggregates, the matrix has all zeros. When a square-shaped aggregate is to be generated, the program first creates a small matrix of the size of the aggregate with all ones, then checks if the assigned position in the concrete matrix have any non zero values. If so, there is conflict and the program tries a new position; otherwise all pixels in the assigned area are changed to ones, and the new aggregate is generated.

2.2.4 Polygon-shaped aggregates

Polygon shapes are more realistic than circles and squares for simulation of coarse aggregates. A simple way to generate non-overlapping polygons is to use inscribed polygons in circles that have been generated in circle-shaped aggregate models. For each circle with a specified radius r and the center coordinates (x_o, y_o), a random integer from 3 to 10 assigns the number of polygon sides, and another set of n random numbers between 0 to 2π in ascending order give the inscribed angles for each vertex

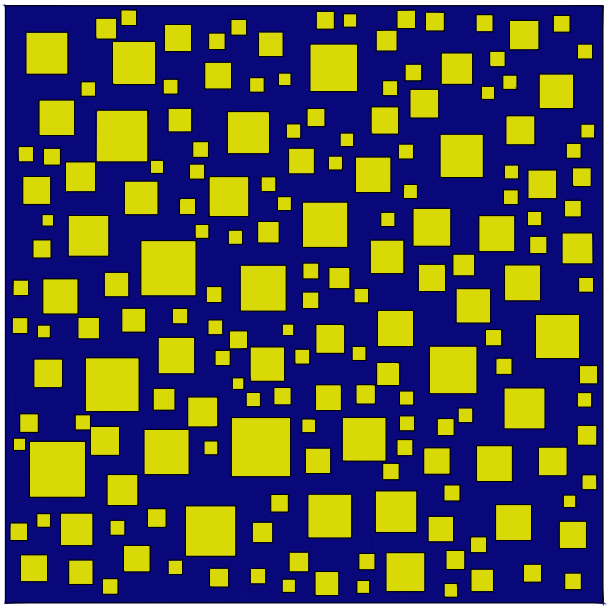

Figure 2.3: Randomly distributed square-shaped aggregates placed in a 15 cm×15 cm concrete model with volume percentage 35%.

(figure 2.4). The coordinates of each vertex P_i are obtained using the formula

$$x_{P_i} = x_o + r\cos(\alpha_i), \tag{2.2}$$

$$y_{P_i} = y_o + r\sin(\alpha_i),\ i = 1, n. \tag{2.3}$$

This algorithm is very efficient for polygon-shaped aggregate generation. The only drawback is that polygons generated with this algorithm may have large spacing, so it will not reach high aggregate content. Because only coarse aggregates in the size range of 4.75 mm $\sim$ 19.5 mm diameter are modeled, it is reasonable to assume the space between polygons is filled with small aggregates, which are part of homogeneous mortar matrix. The polygon-shaped aggregates are used in all concrete models analyzed in this study.

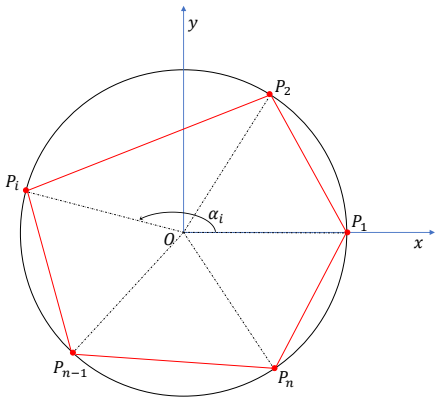

Figure 2.4: Inscribed polygon with random number of sides and vertex positions.

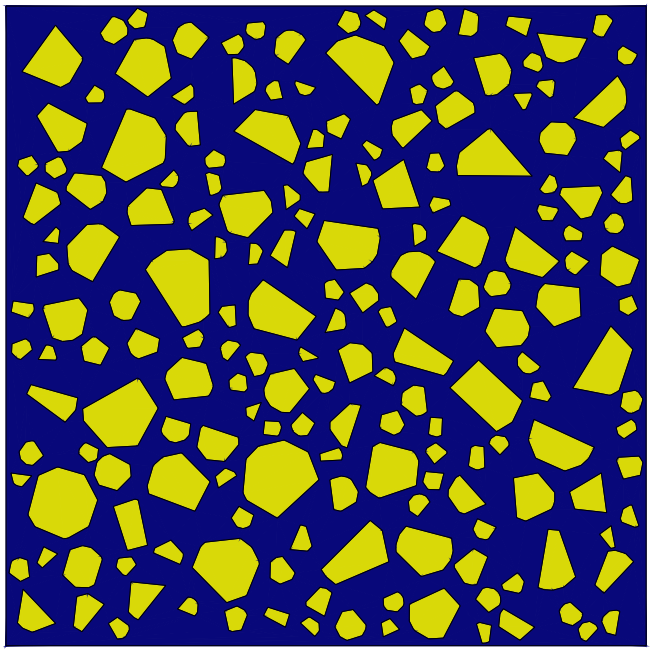

Figure 2.5: Randomly distributed polygon-shaped aggregates placed in a 15 cm×15 cm sample

2.3 Modeling of cracks

Cracks were modeled as ellipses with a very narrow width of 2 mm. The crack lengths were assumed to be randomly distributed in the range of 10 to 20 mm. Parameters needed for simulating a crack include coordinates for the center, major axis of the ellipse (crack length), and an angle in $0 \sim \pi$ for crack orientation. All parameters were

randomly assigned in the specified range. In reality, cracks can overlap or contact with each other to generate a network of connected cracks inside a concrete sample. However for simplicity of modeling, we assumed no overlap or connection among cracks. One simple way to avoid overlapping between cracks is to use the pixel method. First, for a new elliptic crack with the random rotation angle of θ, we use equation 2.4 to obtain the local coordinates of all pixels located inside the ellipse. When this new crack will be placed in the concrete model, the local coordinates of the pixels should be converted to the global coordinates. Then we need to check if there is any conflict between the new crack and existing cracks at the global coordinates. If no conflict, the algorithm changes the values of the matrix at the global coordinates from 0 to 1. Figure 2.6 shows a model with randomly distributed elliptical cracks.

$$\frac{\left((x-x_0)\cos\theta+(y-y_0)\sin\theta\right)^2}{r_1^2}+\frac{\left((x-x_0)\cos\theta+(y-y_0)\sin\theta\right)^2}{r_2^2}=1 \qquad (2.4)$$

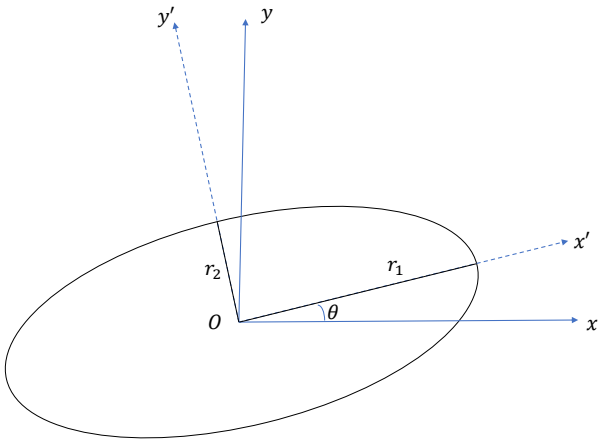

Figure 2.6: Ellipse-shaped crack with random radius and rotation.

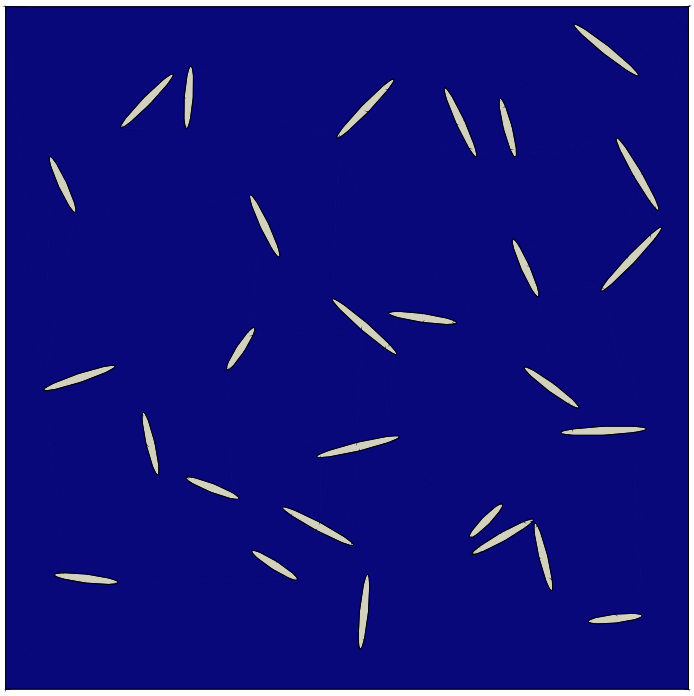

Figure 2.7: Randomly distributed cracks in a 15 cm×15 cm sample.

2.4 Concrete with coarse aggregates and cracks

In order to build a mesoscopic model of concrete with micro-cracking damage, it is necessary to implement both the crack and the aggregate generating algorithms in the finite element model. In this case, it is assumed that cracks can overlap or pass through the aggregates. Therefore in Abaqus, we first generated a concrete model with aggregates in the mortar matrix, and then added cracks to this model. To avoid confliction in material property definition in the crack positions where have been occupied with aggregates or mortar, we need first remove all material at all crack positions, and then merge this modified concrete model with the crack-only model. The final model is shown in figure 2.8.

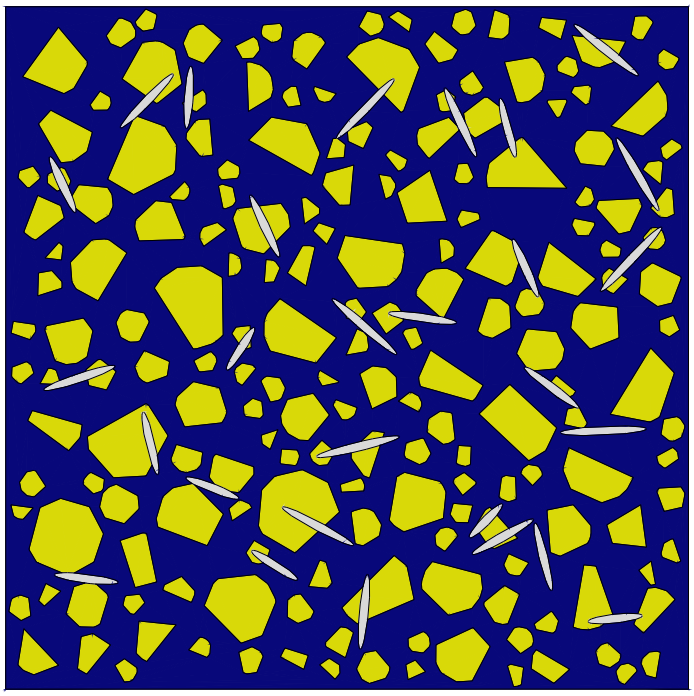

Figure 2.8: Randomly distributed aggregates and cracks in a 15 cm×15 cm concrete model.

2.5 Crack density

A petrographic examination method using the Damage Rating Index (DRI) has been proposed to quantify ASR damages [13, 14]. In this method, a concrete sample with the surface area of at least 200 cm^2 is polished and gridded into 1 cm×1 cm square units. Every unit is then magnified (14-16 x) using a stereomicroscope, and the number of cracks and their respective features are recorded. Based on the petrographic features defined for each crack type, each crack gets a weighting factor. A DRI value is the multiplication of the crack number by its respective weighting factor, normalized for a 100 cm^2 surface area [13, 14, 15]. Detection and categorization of cracks heavily depend on the operator's experience.

A simple method that avoids these limitations is calculating the crack density solely based on counting the number of cracks caused by ASR reaction [13, 15]. Sanchez [13]

found that the crack density increases as a function of the specimen's expansion level. Therefore, in this study, the crack density parameter is used to quantify microcracking damage level by counting the number of crack in each 1 cm×1 cm unit and then normalizing its value for a 100 cm^2 surface area. This can also be done by summing up the total crack lengths and normalizing the length by the area. We performed analyses on 4 models with different stages of damage with crack densities of 0, 0.07, 0.13, 0.19 and 0.26 $/cm^2$ respectively. Wave propagation analyses are performed on these models to investigate how microcracking damage affects the measuring signal in each stage.

2.6 Material properties

In this research, four different material properties were investigated to model concrete with induced cracks. Cracks were initially assumed to be filled with air to simulate open cracks. Since ASR is one of the major types of damages in concrete, we also simulated cracks filled with the ASR gel product. Finally, in the last stage of our analyses, we assumed ASR gel only presents in cracks generated within aggregates. These cracks are separated in two parts where the section in aggregates is filled with the ASR gel material, and the part inside mortar is filled with the air properties. All the materials are considered to be isotropic and homogeneous. Material properties of aggregate and mortar are extensively studied, however there are very few sources that studied the mechanical properties of the ASR gel [16, 1]. Values used for ASR gel properties in this research are based on the average mechanical properties measured by Moon et al. [1].

Figure 2.9: Image of an ASR gel fragment collected from the Furnas dam [1]

Mechanical properties of aggregates, mortar, air and ASR gel, used in these models are shown in table 2.1, where ρ is density, E is elastic modulus, ν is Poisson's ratio, and K is bulk modulus.

Table 2.1: Material Properties used in numerical simulation

Material	ρ (kg/m^3)	E(GPa)	ν	K(GPa)	V_p(m/s)	V_s(m/s)
Mortar	2200	30	0.22	17.9	3946	2364
Aggregate	2700	70	0.22	41.7	5441	3260
ASR gel	2060	25	0.35	27.8	4413	2120
Air	1.2	-	-	1.00E-04	293	-

2.7 Material damping

In order to simulate the wave attenuation in concrete, a Rayleigh damping model is utilized. Rayleigh damping model assumes the damping matrix as a function of the mass (M) and the stiffness matrix (K) (Eq. 2.5).

$$C = \alpha M + \beta K \tag{2.5}$$

Here, α and β are Rayleigh damping factors that can be used as inputs in the finite

element analysis software. There are different methods [17, 18, 19] to calculate theses factors for heterogeneous materials like concrete. Tian et. al. [17] placed a transducer and multiple receivers inline with each other, and suggested that the amplitude change in receiving signals from different receivers is a function of distance from the source, geometrical spreading and attenuation coefficients (Eq. 2.6):

$$W_2 = W_1(\frac{r_1}{r_2})^n e^{-K_w(r_2-r_1)} \tag{2.6}$$

Taking the natural logarithm of both sides of the Eq. 2.6, a linear relation between the attenuation factor(K_w) and the ultrasonic wave amplitudes from two receiving signals can be found. A linear regression can be used to find the wave attenuation in the medium.

Rayleigh damping factors (α and β) can be calculated using Eq. 2.7 where c_L is wave velocity travelling inside the material and ω is the angular frequency. α for normal concrete is usually between 2000-2200 and the β can be somewhere from 10^{-8} - 10^{-6}. It should also be noted that in higher frequencies (f >1 kHz) the mass damping factor (α) has less effect on overall Rayleigh damping. In this thesis, we defined $\alpha = 2120$ and $\beta = 1.787 \times 10^{-7}$.

$$K_w = \frac{\alpha}{2c_L} + \frac{\beta}{2c_L}\omega^2 \tag{2.7}$$

2.8 Input force

Scattering of an ultrasonic wave caused by aggregates and cracks inside a concrete sample is strongly affected by its wavelength. When the wavelength is in the order of the aggregate and crack size, the wave can interact with multiple scatterers before

reaching the receiver. Assuming a constant value for wave velocity in a homogeneous space, the wavelength is inversely proportional to the frequency. In order to simulate waves of different frequencies, we defined transient loads in the form of squared half-sinusoidal functions (Eq. 2.8). For duration T of 10 μs, 25 μs, 40 μs, 50 μs, 75μs and 100 μs, the force histories are shown in figure 2.10. The half-sinusoidal function is squared to avoid the abrupt changes of amplitude at the beginning and end of the input force periods that could be troublesome for numerical simulations.

$$f(t) = \sin^2(\frac{\pi t}{T}) \tag{2.8}$$

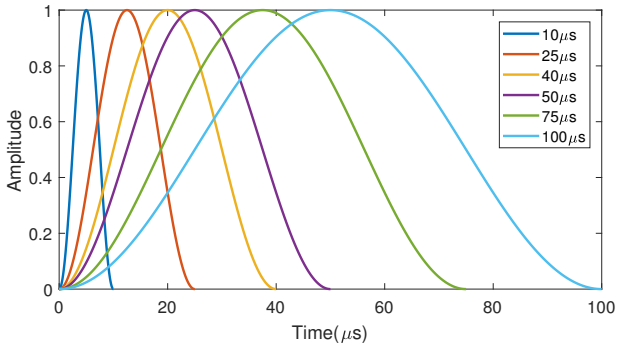

Figure 2.10: Input force functions with different time duration

2.9 Element type, mesh, and boundary conditions

We choose Abaqus©/Explicit as the finite element analysis software. The mesh size and the time step are two important factors in numerical simulation of wave propagation in material. If the mesh size and time step are too big the numerical model will show large errors comparing with the analytical solutions. On the other hand selecting too small values for the mesh size or time step can increase the processing time drastically and increase the computation cost. In order to choose the right values for the mesh size and time steps, it should be noted that the highest wave frequency affects the times step while the shortest wavelength is responsible for the mesh size

[20]. The ideal mesh size should be $1/10 \sim 1/20$ of the shortest wavelength [21, 22, 20]. Here, The plane strain element CPE3 is used to mesh the model with size of 1 mm for input force duration of 25 μs and higher, and 0.5 mm for force duration of 10 μs. The selected mesh sizes are smaller than 1/20 of the shortest wavelengths. A demonstration of meshed model with 1 mm mesh size is shown in figure 2.11. Another rule of thumb for assigning an efficient time step is the smallest wave period should be at least $10 \sim 20$ larger than the selected time step[20]. Time steps of 1 μs for the models with the force duration of 25 μs and higher and 0.5 μs for the model with the input force duration of 10 μs is selected here. To validate the mesh size and time steps used in this research, a bench mark simulation of wave propagation in fluid-solid half-space was performed and the results were in conformity with the analytical result by Zhu et al. [23].

Wave scattering can be caused by coarse aggregates, cracks and sample boundaries. Using a large model may reduce or delay reflections from boundaries; however it will cause a significant processing cost due to the size of the model. Instead, in a small model, waves can reach the boundaries very quick, and generate multiple boundary reflections in the concrete medium and diffuse really quick. In this study we modeled a 15 cm$\times$15 cm concrete sample and to ensure the stability of the model, two hinge supports were placed at two bottom corners of the model.

The excitation source is located on the top surface in the middle (7.5 cm from the left), and the receiver is located at the middle of the bottom surface.

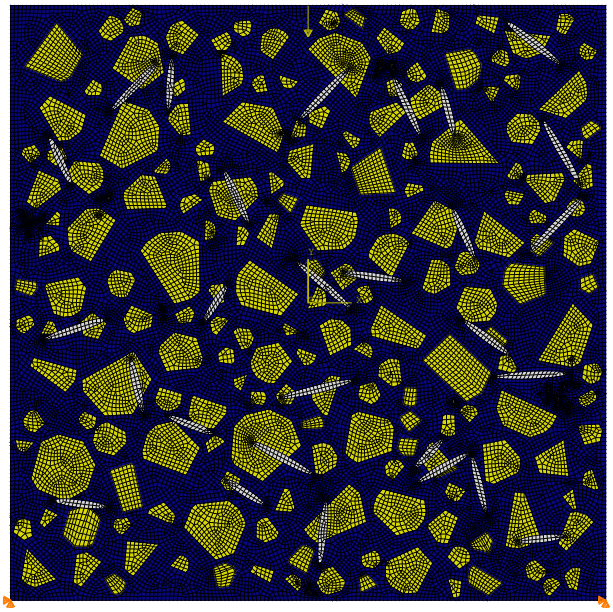

Figure 2.11: Meshed concrete model with coarse aggregates and cracks.

2.10 Parametric analysis

Since the objective of this research is to investigate effects of microcracking damage in concrete on ultrasonic signals, models corresponding to 4 different damage stages were selected for simulation. These models have increasing crack densities of 0.07, 0.13, 0.19 and 0.26 count/cm^2. Then effects of other parameters including aggregate angularity, aggregate content, crack material properties and input force frequency were also studied. To study the effect of wave frequency, we selected three different input loads with the same amplitude but different duration times (10 μs, 25 μs, 40 μs, 50 μs, 75 μs and 100 μs). For aggregate content effect, three different aggregate contents (base model with 35% aggregate content by volume comparing to the models with 30% and 25%) were investigated. In order to simulate different types of cracks - open cracks and ASR induced gel filled cracks, three different combinations of material properties, air, ASR gel, and a combination of air and ASR gel were studied. This extensive collection of models with different parameters would help us understand the effects of each parameter through numerical simulation.

CHAPTER 3

Numerical Simulation Results

3.1 Simulated wave field

Figures 3.1-3.3 present snapshots of wave field at 30 μs in a homogeneous medium, concrete, and concrete with air-filled cracks. The input force duration is 25 μs. For the homogeneous medium, there are clear circular wavefronts for P and S waves. Rayleigh wave is also observed near the surface. In concrete with coarse aggregates, P and S wavefronts are distorted by aggregate scattering, but they are still discernible. In the concrete model with air-filled cracks, diffuse wave field forms due to strong wave scattering by cracks.

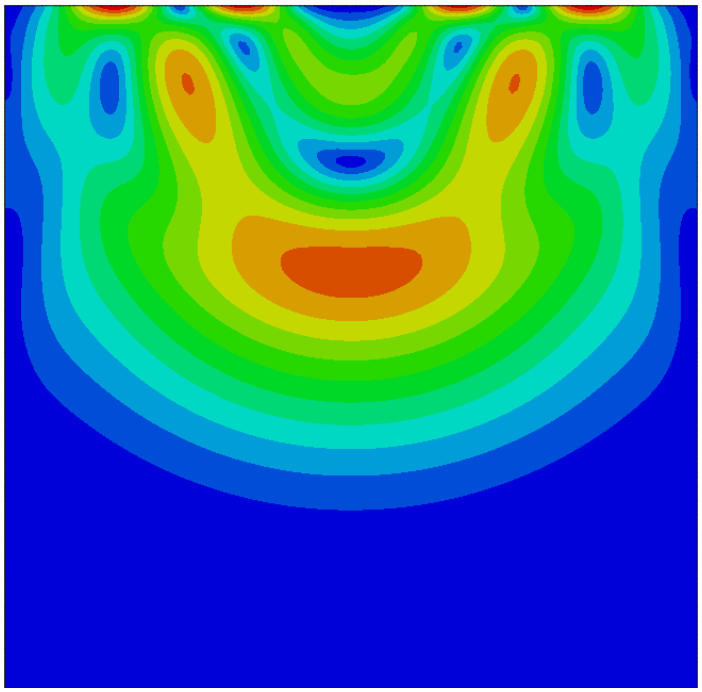

Figure 3.1: Snapshot of wave field in a homogeneous medium at 30 μs. Input force duration is 25 μs.

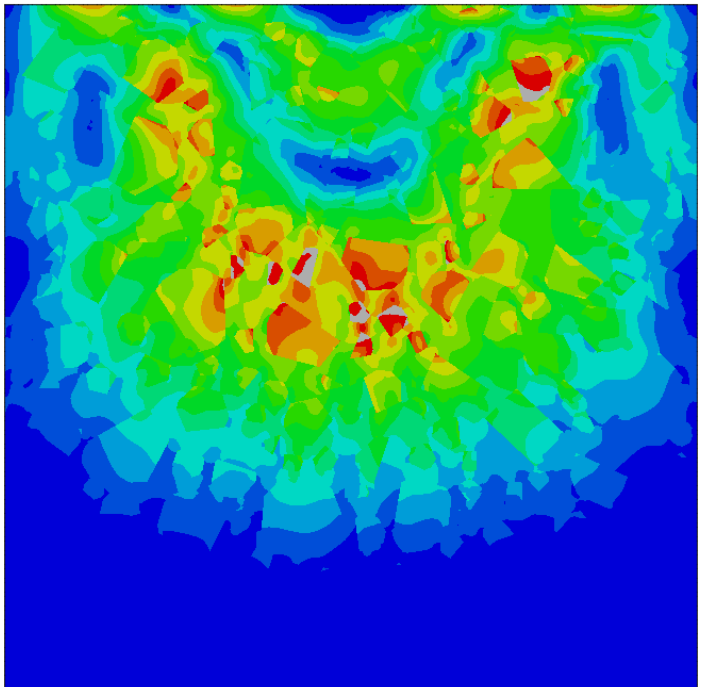

Figure 3.2: Snapshot of wave field in concrete with coarse aggregates at 30 μs.

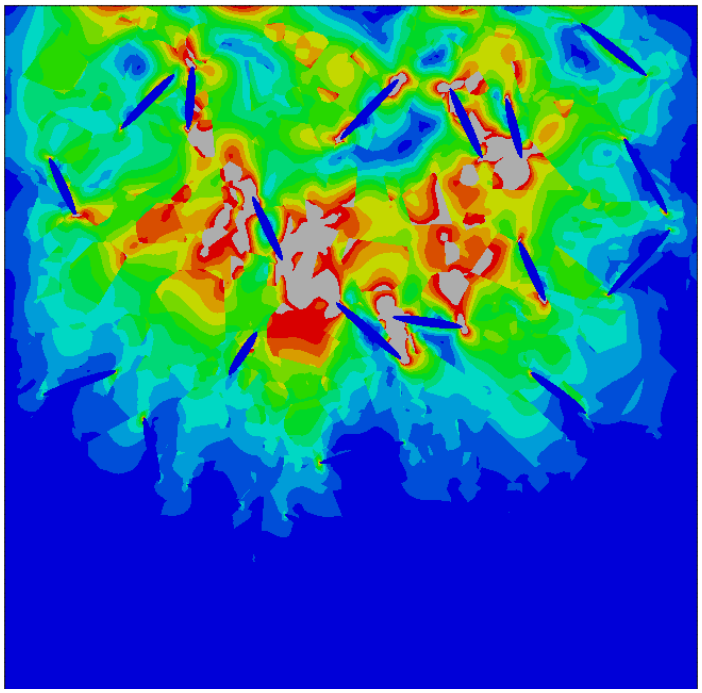

Figure 3.3: Snapshot of wave field in concrete with coarse aggregates and air-filled cracks at 30 μs.

3.2 Coda wave analysis

Coda Wave Interferometry (CWI) is a wave analysis technique by comparing the tail part of signals (Coda) before and after a perturbation in a highly scattering media and calculating the relative wave velocity change between signals. For minimal changes in a medium, the first arrivals may not show detectable difference. However, because the Coda is scattered and reflected multiple times by the heterogeneities and has propagated a long distance before reaching the receiver, it can show high sensitivity to minimal changes in the medium, including new scatters such as microcracks, stress or temperature changes. Figure 3.4 shows two ultrasonic signals measured in a concrete sample at different temperatures. In the later part of signal (>0.4 ms), clear difference is observed between the signals, while this change cannot be accurately measured in the early part of signals (<0.1 ms).

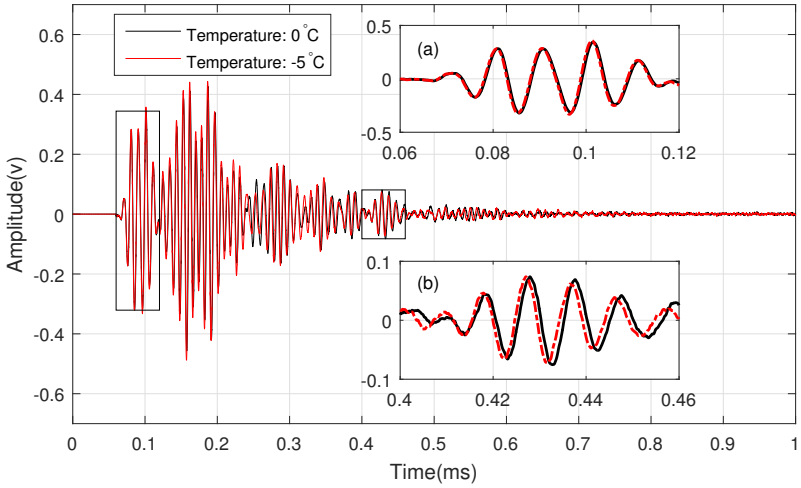

Figure 3.4: Coda waves of two ultrasonic signals measured at different temperatures.

CWI analysis can be used to obtain the relative velocity change between two signals [24, 25]. Two commonly used methods are the doublet and the stretching methods. In the doublet method, a signal is divided into multiple small overlapping time windows of length T with window centered at t_i, and the cross-correlation between the reference

and disturbed coda waves is calculated by using the formula 3.1. For each window, the time delay dt_i that maximizes the cross-correlation is plotted vs. the window position t_i. The slope of the dt vs. t curve gives the relative velocity change dV/V in the medium [26].

$$CC(t, \delta t) = \frac{\int_{t-T/2}^{t+T/2} \varphi(t)\acute{\varphi}(t+\delta t)dt}{\sqrt{\int_{t-T/2}^{t+T/2} \varphi^2 dt \int_{t-T/2}^{t+T/2} \acute{\varphi}^2 dt}} \tag{3.1}$$

$$\delta t/t = -\delta v/v \tag{3.2}$$

The stretching technique assumes uniform velocity change in the medium, therefore two signals can be compared by stretching or compression. The cross-correlation coefficient is calculated between the reference and the stretched (or compressed) version of disturbed signals using Eq. 3.3, where φ and φ' are the signals before and after perturbations and T is the length of the signal window used for the analysis. The stretching (or compressing) factor that maximizes this correlation coefficient is equal to relative velocity change between two models [27, 25].

$$CC(\varepsilon) = \frac{\int_{t-T/2}^{t+T/2} \acute{\varphi}\left[t(1-\varepsilon)\right]\varphi(t)dt}{\sqrt{\int_{t-T/2}^{t+T/2} \acute{\varphi}^2\left[t(1-\varepsilon)\right] dt \int_{t-T/2}^{t+T/2} \varphi^2(t)dt}} \tag{3.3}$$

$$\varepsilon_{max} = \delta v/v \tag{3.4}$$

Since the stretching method can use the whole signal window and the velocity change values calculated with this method are not dependent on the number of time windows or their overlapping factor, in comparison with the doublet method, it can give more stable results.

3.3 Wave diffusion approximation

An ultrasonic wave traveling through a heterogeneous medium like concrete can be subject to a large number of scatterings if the wavelength is in order of the aggregates sizes. These scatterings can cause a rapid changes in the amplitude, phase, or the path of the propagating wave, which ultimately results in the wave attenuation. The attenuation due to the heavy scattering inside the concrete generates a diffuse wave field. The ultrasound energy field diffusion in concrete can be defined as a function of diffusivity and dissipation parameters. The diffusivity is mainly reflective of material structure such as the aggregate content or their placements in the concrete while the dissipation mostly depends on the viscoelastic properties of the cement paste [4, 28, 5] .

The diffusion of ultrasonic energy in concrete can be modeled by the two-dimensional diffusion equation with dissipation [5, 6]. This equation can be given as

$$D(\frac{\partial^2}{\partial x^2}+\frac{\partial^2}{\partial y^2})\left\langle E(x,y,t)\right\rangle-\frac{\partial}{\partial t}\left\langle E(x,y,t)\right\rangle-\sigma\left\langle E(x,y,t)\right\rangle = E_0\delta(x-x_0)\delta(y-y_0)\delta(t-t_0) \tag{3.5}$$

where E_0 is the initial spectral energy of the ultrasonic wave coming from the source at $x = x_0$, $y = y_0$ and time $t = 0$, D is ultrasonic diffusivity(unit m^2s^{-1}) and σ is dissipation(unit s^{-1}). The solution of Eq. 3.5 is given by

$$\left\langle E(x,y,t)\right\rangle = \frac{E_0}{4D\pi t}e^{-(x^2+y^2)/(4Dt)}e^{-\sigma t} \tag{3.6}$$

Taking the natural logarithm of Eq. 3.6, results in

$$ln\left\langle E(x,y,t)\right\rangle + lnt = C_0 - \frac{(x^2+y^2)}{4Dt} - \sigma t \tag{3.7}$$

where $C_0 = ln(E_0/4\pi D)$. In order to calculate the diffusion and dissipation, first, the

spectral energy of the receiving signal should be calculated. For this purpose, the time domain response is divided into overlapping windows of length δt. Next, a discrete-time Fourier transform for each time window is calculated and squared. Having the spectral energy and their respective time (center time of each time window), a polynomial regression of second degree is used to fit the data made based upon Eq. 3.7. The first and the third polynomial factors from the polynomial regression fit can be used for calculating the diffusion and dissipation for each signal.

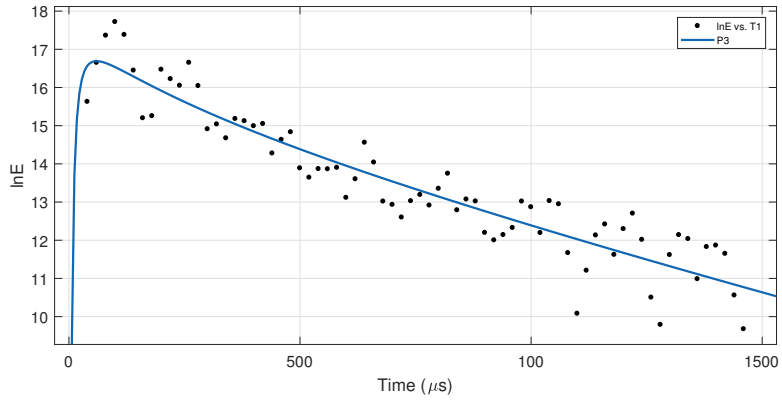

Figure 3.5: Spectral energy vs. time (the solid line is a curve fit to the two-dimensional diffusion equation).

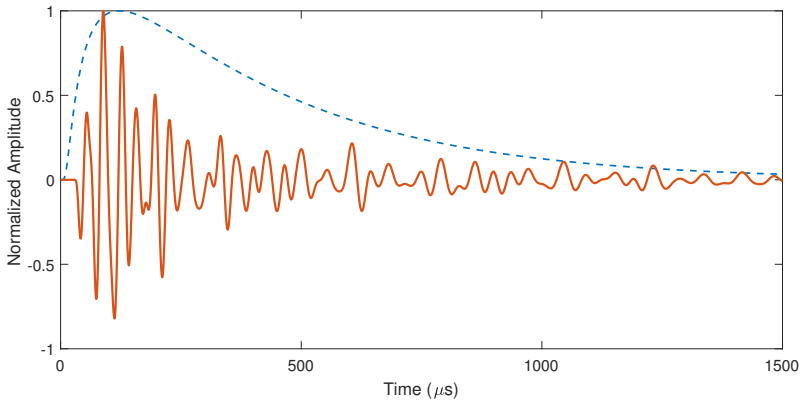

Figure 3.6: Normalized time domain signal with diffusion envelope (dashed line).

3.4 Effect of aggregate

3.4.1 Aggregate angularity

Figure 3.7 shows the comparison between three concrete models with different aggregate shape and angularity. The three models have the same aggregate content, aggregate placement, crack density and input force function. The aggregate content is 35% by volume, crack density is 0.19 $/cm^2$ and the input force duration is $25\mu s$. Figure 3.8 presents the receiving signals from all three models. CWI analysis of these signals shows that the velocity change in this case is less than 0.1%. The diffusion analysis also shows a very small variation in both diffusion and dissipation factors between the three models. Therefore, it can be concluded that variation of aggregate angularity does not have a considerable effect on ultrasonic wave propagation. Study by Asadollahi and Khazanovich [12] validates the nominal effect of the aggregate shape on the received signal.

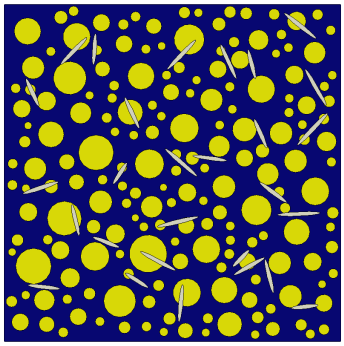

(a) Model with circular shape aggregate

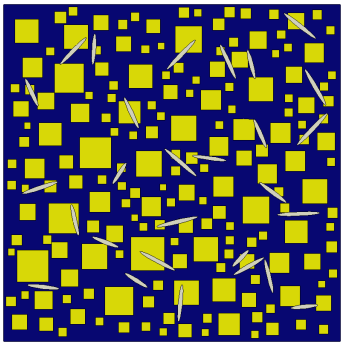

(b) Model with square shape aggregates

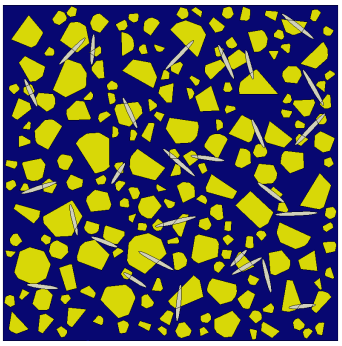

(c) Model with polygon shape aggregates

Figure 3.7: Concrete models with different aggregate contents.

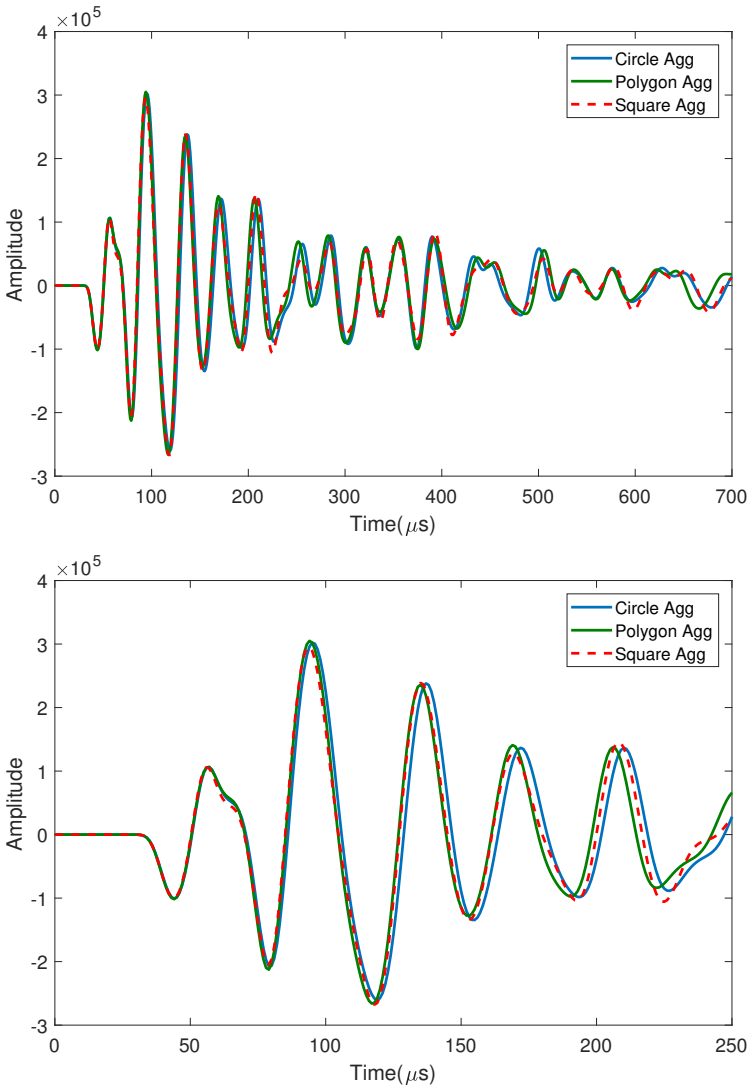

Figure 3.8: Aggregate angularity effect on received signals in concrete models with the same aggregate content and crack density

3.4.2 Aggregate content

Figure 3.9 shows the comparison between three concrete models with different aggregate contents. The base model has the aggregate content of 35%, and the two other models each contain 30% and 25% aggregate.

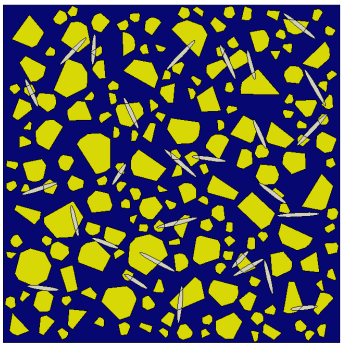

(a) Model with 35% aggregate content

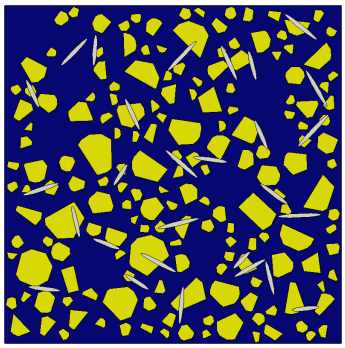

(b) Model with 30% aggregates content

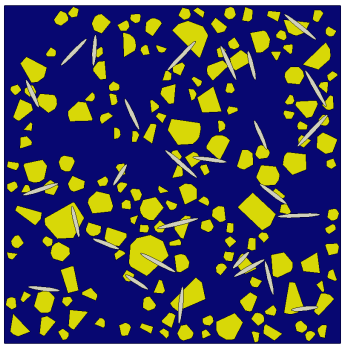

(c) Model with 25% aggregates content

Figure 3.9: Concrete models with different aggregate contents.

Figure 3.10 presents the receiving signals from the three models. CWI analysis shows that the relative velocity decrease from the 35% model to the 30% model is less than 0.7%. However, the velocity decrease from the 30% model to the 25%, shows a much larger value of 2.9% . The dissipation factor from the diffusion analysis also shows a similar pattern where the dissipation is 2670 (1/s) for the 35% model, 2810 (1/s) for the 30% aggregate model and 3884 (1/s) for the 25% model. Both velocity

change and dissipation factor results suggest that by removing more aggregate the rate of both velocity change and dissipation increase considerably. Since the damping factors are only defined on the mortar part, by replacing more aggregates with mortars we are actually increasing the overall damping and attenuation in the model which results in the increase of the dissipation. Also, since the mortar has lower impedance than the aggregates, by removing the aggregates the velocity decreases.

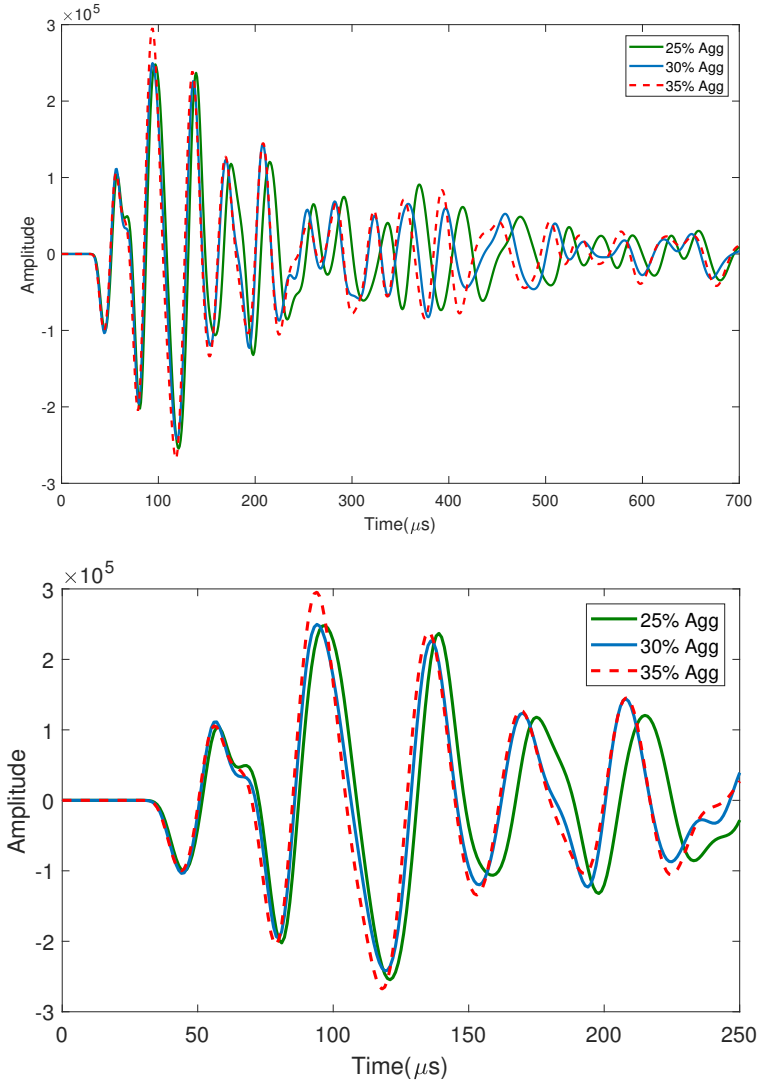

Figure 3.10: Aggregate content effect on received signals in concrete models with the same crack density

3.5 Effect of cracks

3.5.1 Material properties of cracks

Cracks can be assumed to be filled with either air or ASR gel (figure 3.11a and figure 3.11b). However, this assumption is not very accurate in reality. Once ASR occurs, the generated expansive gel causes tension and cracking in concrete, and the gel fills in cracks. Therefore, a reasonable assumption should be cracks to be partially filled with the ASR gel. Cracks inside or around aggregates are filled with ASR gel, while cracks in the mortar part are filled with air (open cracks). Figure 3.11c shows a more realistic model of ASR-induced cracks in concrete based on this assumption.

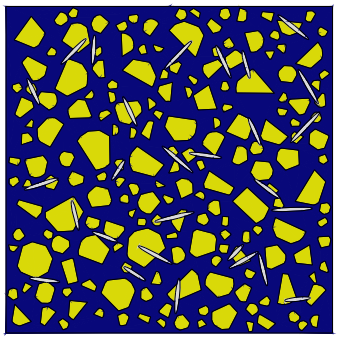

(a) cracks filled with air

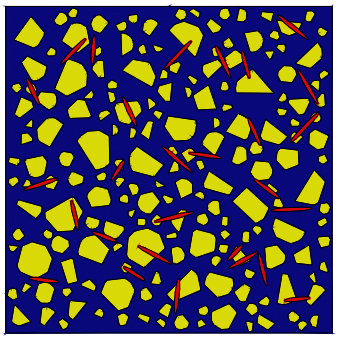

(b) cracks filled with ASR gel

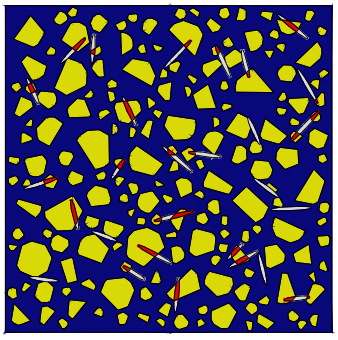

(c) cracks with both ASR gel (inside aggregates) and air (inside mortar)

Figure 3.11: Concrete models with the same aggregate content and different crack properties.

Figure 3.12 presents the received signals from the three crack models. The input

force duration here is 25 μs. For the gel-air crack model, its amplitude and first arrival are between the responses of complete air-filled and complete gel-filled, and closer to the air-filled model response. By performing the CWI analysis on all three models, we found the relative velocity change between the gel model and 2-part crack model has 6% decrease and from the gel model to the air model we have about 13% velocity decrease. Since the air has much lower acoustic impedance than solids by increasing the air content the wave velocity in the concrete model shows a noticeable decrease .

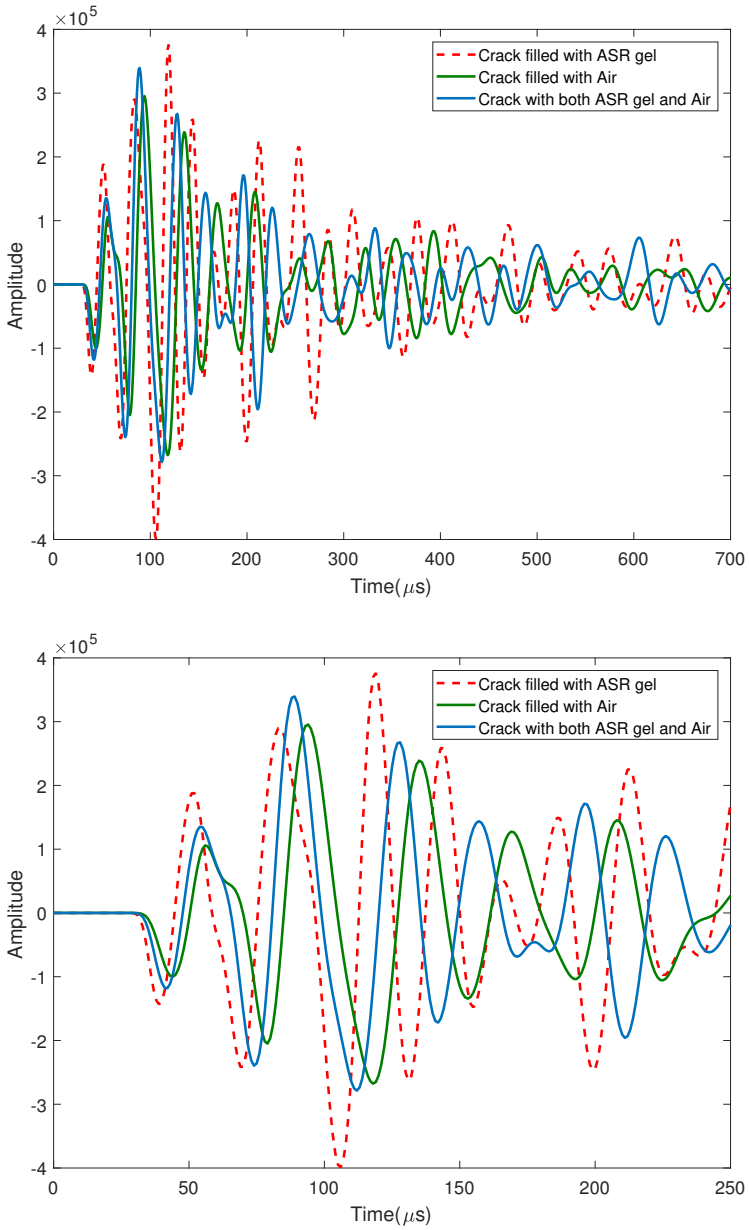

Figure 3.12: Received signals from models with different crack properties

3.5.2 Crack density

Figure 3.13 present four concrete models in different damage stages where the crack density increases in each stage. The cracks are simulated as air-filled in mortar part and gel-filled in aggregate part. Crack densities in these models are $0.07/\text{cm}^2$, $0.013/\text{cm}^2$, $0.19/\text{cm}^2$ and $0.26/\text{cm}^2$ respectively. These models are used to study the effects of crack density on wave velocity change. Results from this analysis will be used as a reference for quantifying microcracking damage in concrete using ultrasonic waves.

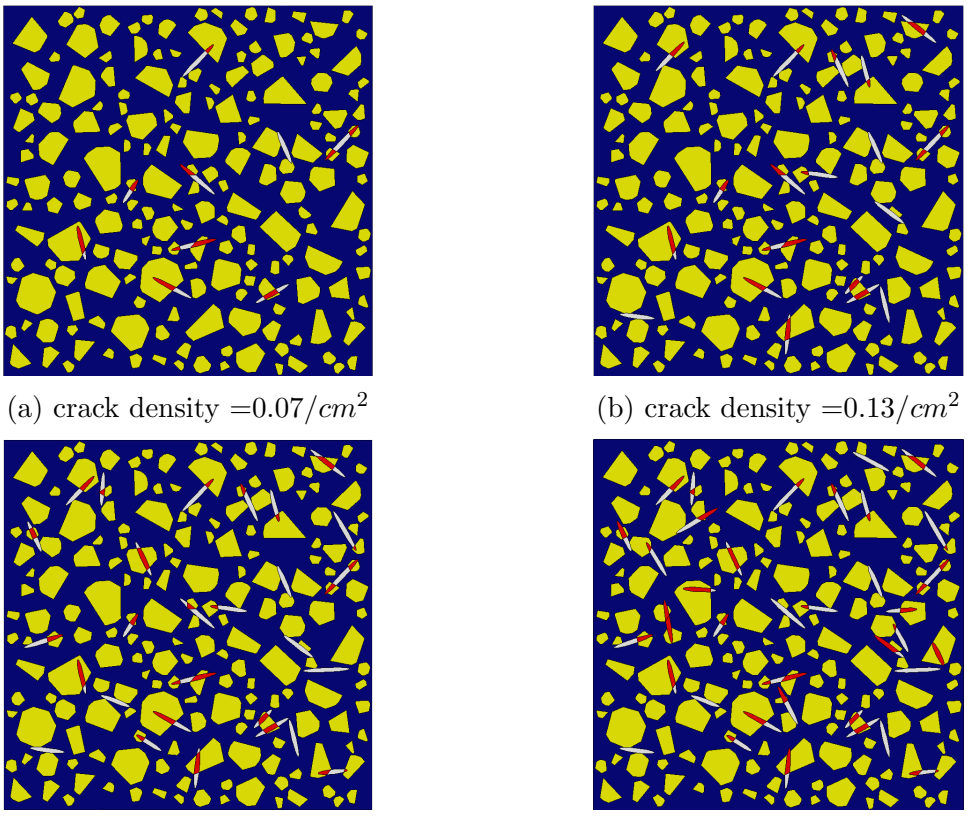

(a) crack density $=0.07/cm^2$ (b) crack density $=0.13/cm^2$

(c) crack density $= 0.19/cm^2$ (d) crack density $= 0.26/cm^2$

Figure 3.13: Concrete models with the same aggregate content (35%) and 4 different crack densities. Cracks are combination of air-filled and gel-filled.

According to figure 3.14, with the increase of the crack density, the signal arrival time increases, and the apparent wave velocity decreases. The relative velocity change can be obtained from the CWI analysis. Figure 3.15 shows the relative velocity change which suggests an almost linear relationship between the relative velocity change and

the crack density. Study by Schurr et al. [11] validates the linear relation between the relative velocity change and the damage.

It should be noted that the crack density parameter in the numerical simulation may under-estimate the actual crack density, and does not fully represent the actual crack network in concrete, however results from these analyses provide us a guidance to relate the relative velocity change with micro-cracking damage levels in concrete.

Figures 3.16 shows the relation between the crack density and the diffusivity. It can be clearly seen that by increasing the crack density the diffusivity decreases. Regarding the dissipation, figure 3.17 shows the relation between the crack density and the dissipation. Although it does not show an evident pattern, the dissipation has an overall increase due to the increase of the crack density. The relation between the damage level and diffusion factor has been studied by Deroo et al.[6]. Their result suggested that with increase of the damage level the diffusivity decreases which can also be clearly seen in fig. 3.16. On the other hand their experimental results from ASR and thermal damages did not show the same relation between the damage level and the dissipation factor. Our results (fig. 3.17) also shows large errors at crack density $= 0.13\ /cm^2$. Further studies on relation between crack density and dissipation may be helpful to address such errors.

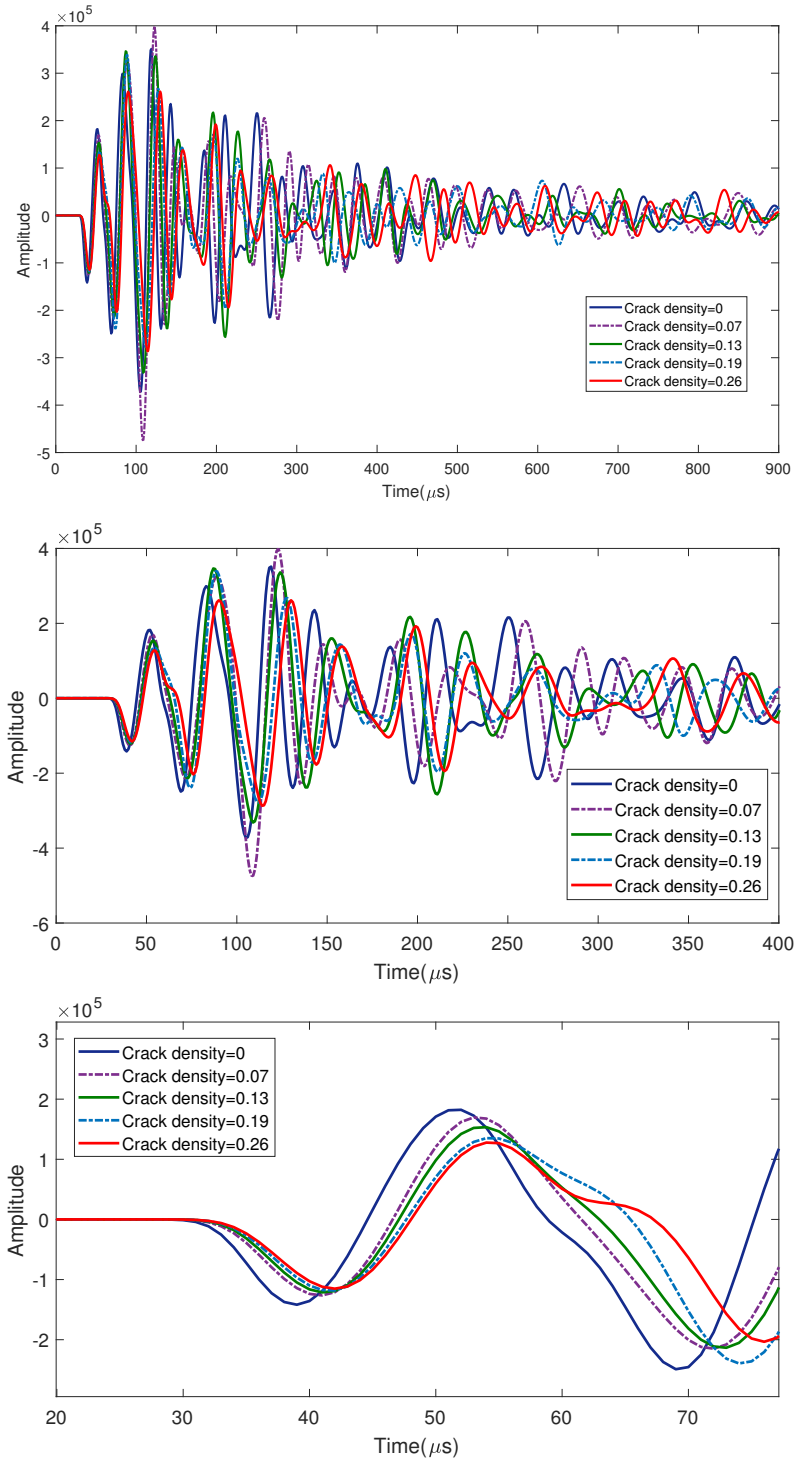

Figure 3.14: Received signals from models with the same aggregate content and different crack densities

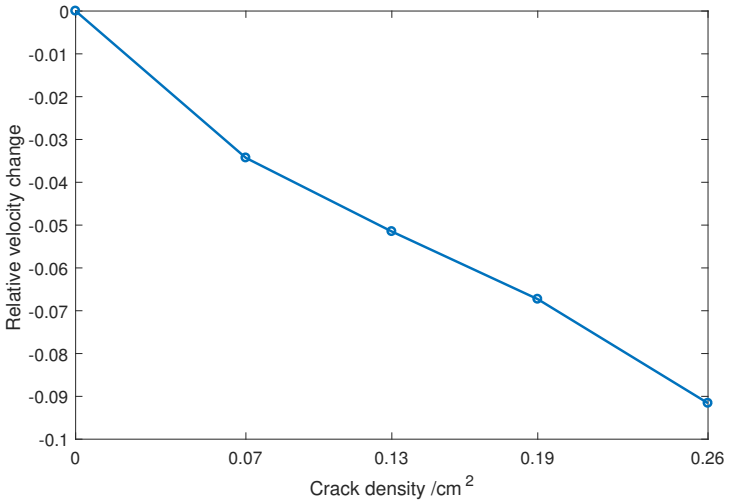

Figure 3.15: Velocity changes due to crack density increase for the 25μs duration input force and gel-air crack properties

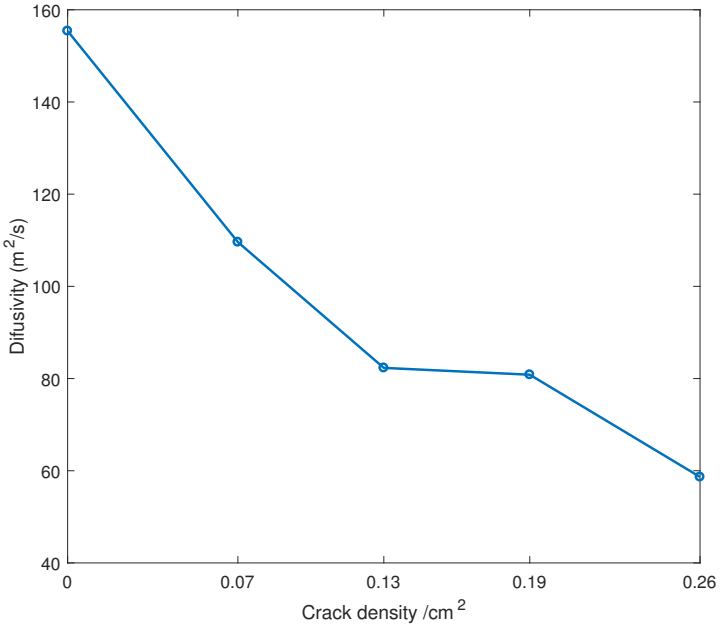

Figure 3.16: Elastic diffusivity due to crack density increase for the 25 μs duration input force and gel-air crack properties

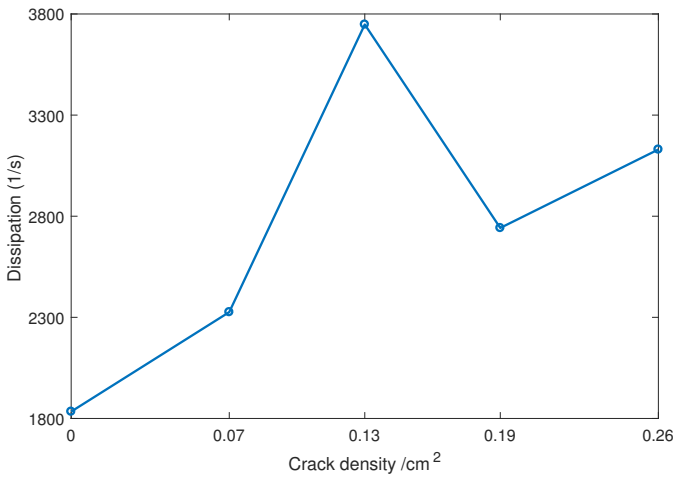

Figure 3.17: Dissipation due to crack density increase for the 25 μs duration input force and gel-air crack properties

3.6 Effect of the input source duration

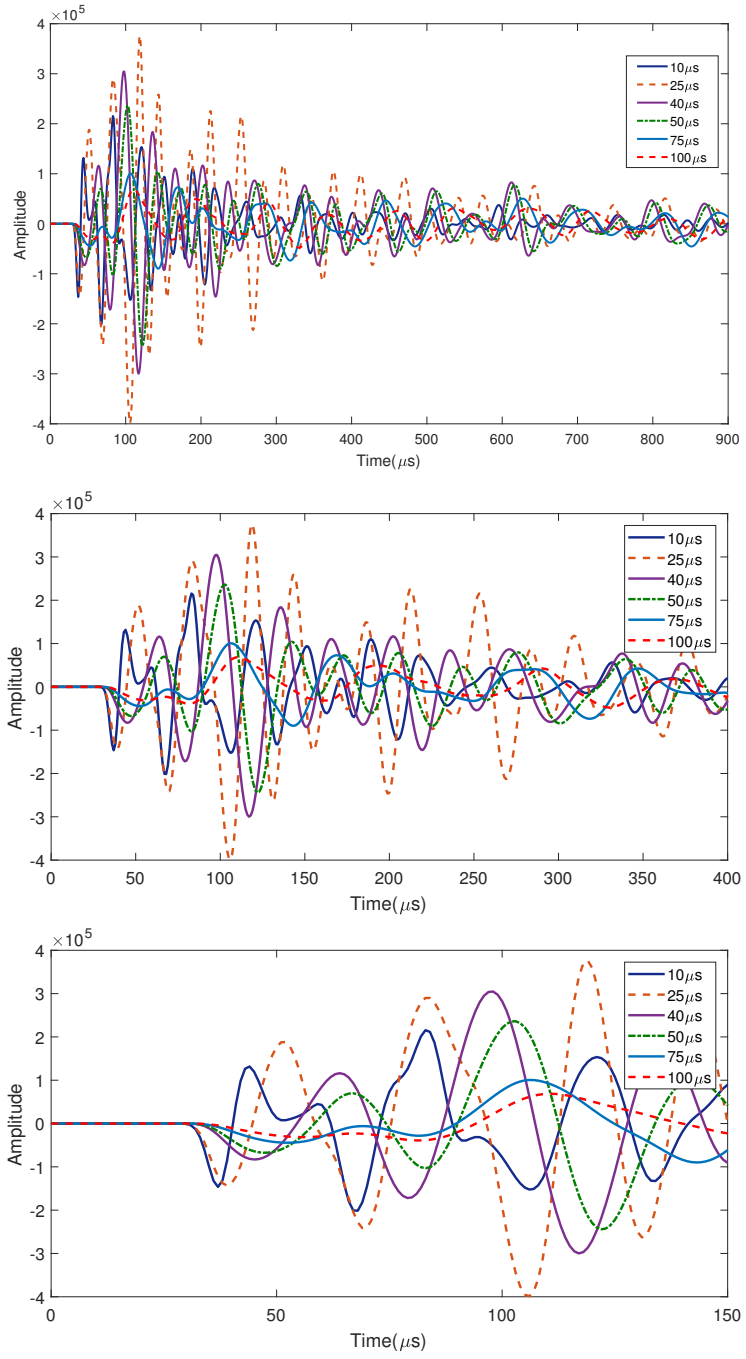

Figure 3.18: Received signals from models with the same crack and aggregate contents and different force input duration

Figure 3.18 presents the received signals on the five concrete models with the same aggregate content (35% aggregate content), the same crack content (0.19 $/cm^2$ gel-

air cracks) and different force duration of 100, 75, 50, 40, 25 and 10 μs. This figure includes 900 and 400 μs long signals and an initial 150 μs segment of the signal to show details regarding the first arrivals. According to figure 3.18, we notice the first wave arrival delays with the the increase of input force duration. Performing a diffusion analysis, figure 3.19 shows an overall decrease in dissipation due to the increase of the input force duration. The higher frequency wave is subject to higher attenuation and dissipation. It should be noted that the coda wave analysis can only be performed when there is a nominal change in the concrete model. However here the model is the same and only the input load has changed. Therefore the coda wave analysis was not utilized here.

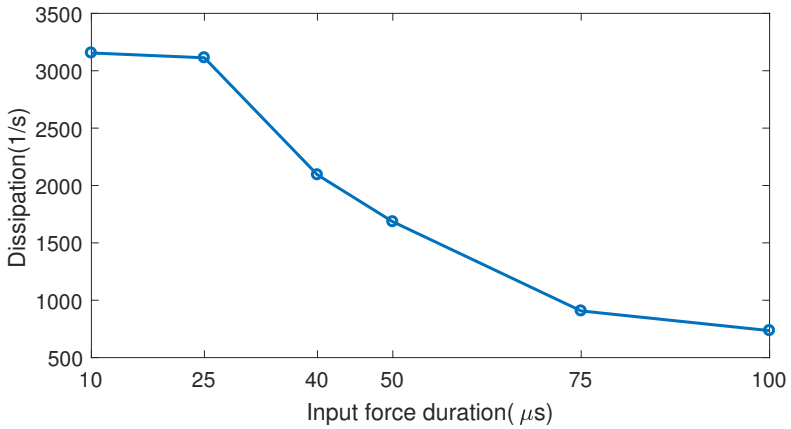

Figure 3.19: Dissipation due to increase of the input force duration in concrete model with 0.19 $/cm^2$ crack density

CHAPTER 4

Conclusions and Future Work

4.1 Conclusions

This thesis presents numerical simulation models and results for diffused wave propagation in concrete with induced cracks. The algorithms for the generation of randomly distributed aggregates and cracks in FEM models were described. With these models, we investigated the effects of different key parameters on wave propagation, including aggregate angularity, aggregate content, crack density, crack properties, and input force frequency.

Analysis results indicate that aggregate angularity has little or no effect on receiving signals. This study suggests that aggregate content change as much as 5% shows only a little effect on velocity, diffusivity and dissipation factors, however an aggregate content change as big as 10% showed more noticeable effect where the velocity change and dissipation had larger increase comparing to the base model.

Crack properties effect on a concrete model with induced ASR cracking was studied. The coda wave analysis suggests that the crack material properties has a large impact on the received signals and three models have considerably large differences. The model with 2-part gel-air cracks has around 6% velocity decrease comparing to the

ASR gel filled crack model. The model with air filled cracks has even a larger velocity decrease of around 13% comparing to the ASR gel filled crack model.

Regarding the crack density, the received signals show that the model with no crack has the earliest first arrival. The CWI analysis suggests that by increasing the crack density, the relative velocity decreases. The diffusivity factor from diffusion analysis also decreases with the increase of crack density. The dissipation, on the other hand, shows an overall increase due to the crack density increase.

Five different input forces with the same amplitude and different durations on similar models with the same aggregate and crack contents were implemented. The dissipation factor from the diffusion analysis suggest that by increasing the input force duration (decreasing the frequency) the dissipation decrease.

4.2 Future work

One suggestion for improving the model is to add the Interfacial Transition Zone (ITZ) layer to the model. ITZ layers have high permeability, and low strength and damages caused by a chemical reaction like ASR can generate a gel that tends to grow and expand in these layers. These types of crackings are multi-scale and multi-physics phenomena with a nonlinear spirit; therefore, in future studies, nonlinear material properties and analysis will be included in numerical simulations.

In this research, our main focus was on the analysis of the wave responses after introducing random cracks inside the concrete. These cracks were not connected and did not grow after each stage. However, in reality, the cracks start to grow and shape a connected network inside the concrete. Therefore a model with a growing crack network can offer a more realistic simulation of damaged concrete.

A 3-D model with randomly placed aggregates and cracks can be computationally expensive. However, this model can result in a more realistic simulation and smaller errors. The 3-D diffusion analysis can also provide better curve fits and as a result, more realistic diffusivity and dissipation factors.

Appendix A

MATLAB source code

The source codes used in this study are presented here. Source codes are based on MATLAB programming. The main program generates the random aggregate shapes and sizes and checks if they have any overlapping with other aggregates (function "checkoverlap") or the defined borders (function "checkborder"). The code first checks the aggregates overlapping based on their circumscribed circle. Next, the "polygon" function generates a random set of coordinates all placed on the circumscirbed circle and connect them to create a polygon aggregate. Once all the polygon aggregates are assigned, the program uses the center and area of each polygon aggregate and generates the equivalent circle and square shape aggregates. Finally, functions "circop", "sqrcop" and "polyop", generate the input codes for the ABAQUS program.

The main source code for generating the random aggregates is presented here.

```
%This program generates a random set of polygon aggregates and place
%them inside the mortar. Based on the center of each polygon and
%their area then it creates the equivalent circle and square shape
%aggregates in another model.
clear all;
%sieve sizes
sieve = [19 12.5 9.5 4.75 2.36 1.18];
dmax = max(sieve)
```

```
fuller= (sieve/dmax).^0.45*100;
passing = fuller;
% maximum aggregate content generated with this method is no more
    than 36\%
vol = 1;
gradation = [sieve;passing]';
%plot fuller curve
plot(sieve,passing)

close all;
sieve = gradation(:,1);
passing = gradation(:,2);
retained = 100-passing; %% mass retained
cum_volpassing = passing*vol/100;%cummulative volume% in total
    concrete vol
cum_volretained = retained*vol/100;%cummulative volume% retained
%Since the pixel method is uttilized here the sample size multiplied
    by 10
%so we have a higher resoultion
H=150;W=150; %sample dimensions
totalarea=H*W;
figure(1);
h0=rectangle('Position',[0 0 W,H],'FaceColor',[0 0 0.4]);
axis equal
axis off
hold on;

%create a random circle and draw if it's inside the rectangle borders
ic = 0;
B = true;
area_placed = 0.0001;
total_area_placed = 0.0001;
for i = 1:10000
index = find (cum_volretained>total_area_placed,1);
```

```
% if area<cum retained vol, find proper sieve size
rmin = sieve(index)/2; rmax = (sieve(index-1))/2;
xmin = rmin; xmax = W-rmin;
ymin = rmin; ymax = H-rmin;

r = rmin+(rmax-rmin)*rand(1,1);
x = xmin+(xmax-xmin)*rand(1,1);
y = ymin+(ymax-ymin)*rand(1,1);
A = checkborder(x,y,r,W,H);
gama = 0;
if A == true
    if ic == 0
        ic = 1;
        xi(i) = x; yi(i) = y; ri(i) = r;
        B = true;
    else
        B = checkoverlap(x,y,r,xi,yi,ri);
        if B == true
        ic = ic+1;
        xi(ic) = x; yi(ic) = y; ri(ic) = r;
        %h2=rectangle('Position',[x-r y-r 2*r 2*r],'Curvature
   ',[1,1],'EdgeColor',mycolor(index-1));
        end
    end
end
if (A&B) == true
% generate the polygon shape aggregate based on its circumscirbed
   circle
[ric,vertices,n] = polygon(x,y,r);
figure(1)
fill(vertices(:,1),vertices(:,2),'y','EdgeColor','y');
area_placed = polyarea(vertices(:,1),vertices(:,2))/totalarea
area_agg(ic) = area_placed;
total_area_placed = total_area_placed+ area_placed
```

```
72 pause(0.01);
73 % Calculate the equivalent radius and side sizes for the circle and
       square
74 % shape aggregates.
75 rcir(ic) = ric;
76 asq(ic) = ric*0.5*sqrt(pi);
77 % save polygon information
78 poly_vert{ic} = vertices;
79 end
80 end
81
82 %plot Circles
83 figure(2)
84 h0=rectangle('Position',[0 0 W,H],'FaceColor',[0 0 0.4]);
85 axis equal
86 axis off
87 hold on;
88 for i = 1:ic
89
90     h2=rectangle('Position',[xi(i)-rcir(i) yi(i)-rcir(i) 2*rcir(i) 2*
       rcir(i)],'Curvature',[1,1],'FaceColor','y');
91
92 end
93 %plot SQUARE
94 figure(3)
95 h0 = rectangle('Position',[0 0 W,H],'FaceColor',[0 0 0.4]);
96 axis equal
97 axis off
98 hold on;
99
100 for i = 1:ic
101
102     h2=rectangle('Position',[xi(i)-asq(i) yi(i)-asq(i) 2*asq(i) 2*asq
       (i)],'FaceColor','y');
```

```
103
104 end
105
106 %This functions generates data needed for circle,square and polygon
    shape
107 %aggregate models in abaqus
108 %Check text files named expcir.txt and expcir2.txt
109 circop( xi,yi,rcir,H);
110 sqrcop( xi,yi,asq,H);
111 polyop( poly_vert,H );
```

The "checkoverlap" function is to check if the circumscribed circle around the new aggregate has overlap with the ones generated before is as follows.

```
1  function [B]=checkoverlap(x,y,r,xi,yi,ri)
2  nc=length(xi);
3  gama=0.15;
4  B=true;
5  for i=1:nc
6      if sqrt((x-xi(i)).^2+(y-yi(i)).^2)<(r+ri(i))+gama.*r;
7      B=false;
8      break;
9      end
10 end
```

The "checkborder" controls if an aggregate has any overlap with the model borders.

```
1  function A=checkborder(x,y,r,W,H)
2  dist=[x,y,W-x,H-y];
3  gama=0.18;
4  if min(dist)<r*(1+gama)
5      A=false;
6  else
7      A=true;
8  end
```

The "Polygon" function generate a random set of corner coordinates based on the canter and radius of the aggregates circumscirbed circle.

```
function [ric,vertices,n]=polygon(x0,y0,r)
poly_A=0;
circle_A=pi*r^2;
for j=1:10
    n=randi([3 10],1,1);
    s=rand(n,1)*2*pi;
    s=sort(s);
    gama=0.001*randn(1,1)+1;
    xn=x0+r*cos(s)*gama;
    yn=y0+r*sin(s)*gama;
    xn(n+1)=xn(1);
    yn(n+1)=yn(1);
    poly_A=polyarea(xn,yn);
    ric=sqrt(poly_A/pi);
    if poly_A>0.45*circle_A % reject very small narrow polygons
        break;
    end
end
vertices=[xn,yn];
```

The "circop", "sqrop" and "polyop" are responsible for generating the ABAQUS input format.

```
function [  ] = circop( xi,yi,rcir,H)

A = [(xi-H/2);yi-H/2];
peripoint=xi+rcir;
B = [(peripoint-H/2);yi-H/2];
C = [A;B]
fileID = fopen('expcir.txt','w');
formatSpec = 'mdb.models[''Model-1''].sketches[''__profile__''].
   CircleByCenterPerimeter(center=( %0.3f , %0.3f ),point1=(%0.3f ,
```

```
    %0.3f)) \n';;
fprintf(fileID,formatSpec,C);
fclose(fileID);

end
```

```
function [  ] = sqrcop( xi,yi,asq,H)
%UNTITLED3 Summary of this function goes here
%   Detailed explanation goes here
modifxi=xi-H/2;
modifyi=yi-H/2;

A = [modifxi-asq;modifyi-asq];

B = [modifxi+asq;modifyi+asq];
C = [A;B];
fileID = fopen('expsqr.txt','w');
formatSpec = 'mdb.models[''Model-1''].sketches[''__profile__''].
    rectangle(point1=( %0.3f , %0.3f ),point2=(%0.3f , %0.3f)) \n';
fprintf(fileID,formatSpec,C);
fclose(fileID);
end
```

```
function [ ] = polyop( poly_vert,H )

%Delete any input file remained from past
if exist('exppoly.txt', 'file')==2
  delete('exppoly.txt');
end

for i=1:size(poly_vert,2)
clear polyv1 polyv2 polyv3 polyv4
polyv1=cell2mat(poly_vert(i));
polyv2=polyv1-H/2;
    for j=1:size(polyv2,1)-1
```

```
13          polyv3(j,:)=polyv2(j+1,:);
14      end
15  polyv4=[polyv2(1:size(polyv2,1)-1,:) polyv3];
16  fileID = fopen('exppoly3.txt','a');
17 formatSpec = 'mdb.models[''Model-1''].sketches[''__profile__''].Line(
       point1=( %0.3f , %0.3f ),point2=(%0.3f , %0.3f)) \n';
18 fprintf(fileID,formatSpec,polyv4');
19 fclose(fileID);
20 end
21
22 end
```

Appendix B

ABAQUS modeling

ABAQUS scripting is a powerful tool based on Python programming that can be used to generate a model. ABAQUS also offers a Macro tool that can save the user activities while using the graphical user interface (GUI) and can generate the python input that can generate the same model. In an ABAQUS input code, we can assign the geometry, material properties, load inputs, mesh sizes, and many other features. However, in this research, we decided to only use the scripting tool to generate the aggregates and use the GUI for defining other features of the model. In order to create a model with random shape and size aggregates, we started by generating a sample code for a simple model with only one aggregate and then edited it by adding the aggregate coordinate generated by the MATLAB code we described earlier. In ABAQUS, a circle shape aggregate is defined by its center and radius. The square shapes can be defined by coordinates of two point on a diagonal and polygons are defined as a series of lines that create a confined space.

In the following a simple ABAQUS input code that can be used for aggregate generation is presented.

```
from part import *
from material import *
from section import *
from assembly import *
```

```
from step import *
from interaction import *
from load import *
from mesh import *
from optimization import *
from job import *
from sketch import *
from visualization import *
from connectorBehavior import *
mdb.models['Model-1'].ConstrainedSketch(name='__profile__', sheetSize
    =1000.0)

##############

##MATLAB OUTPUTS SHOULD BE INSERTED HERE##

##############
mdb.models['Model-1'].Part(dimensionality=TWO_D_PLANAR, name='Part-1'
    , type=
     DEFORMABLE_BODY)
mdb.models['Model-1'].parts['Part-1'].BaseShell(sketch=
     mdb.models['Model-1'].sketches['__profile__'])
del mdb.models['Model-1'].sketches['__profile__']
```

Once the aggregates and cracks geometries are imported in ABAQUS, the combination can be done using the ABAQUS GUI.

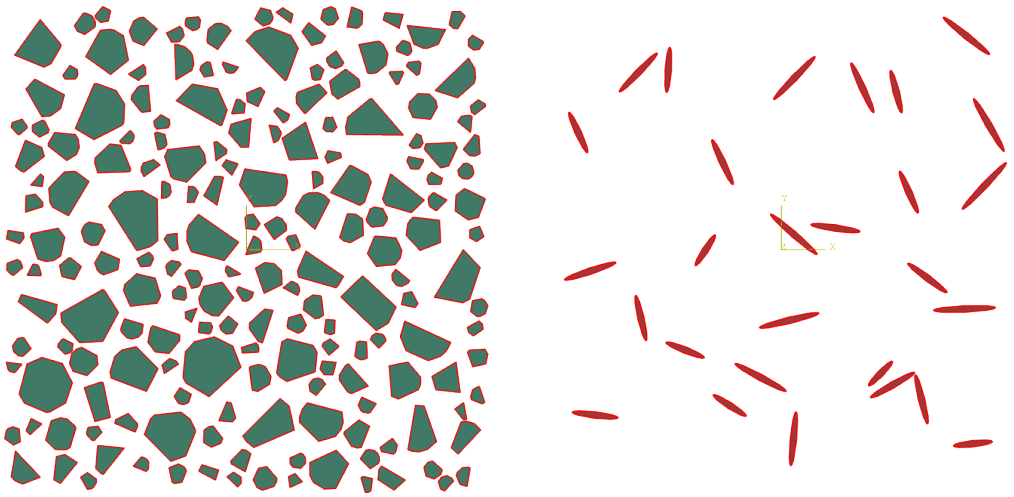

Figure B.1: Aggregates and Cracks geometries imported in the ABAQUS

Figure B.1 shows the two parts imported in ABAQUS. Now we can assign a section with the desired material properties for each part. Next, the crack positions should be removed from the aggregate part to avoid any confliction in material property definition and then when we can merge the two parts together and create a part with both cracks and aggregates.

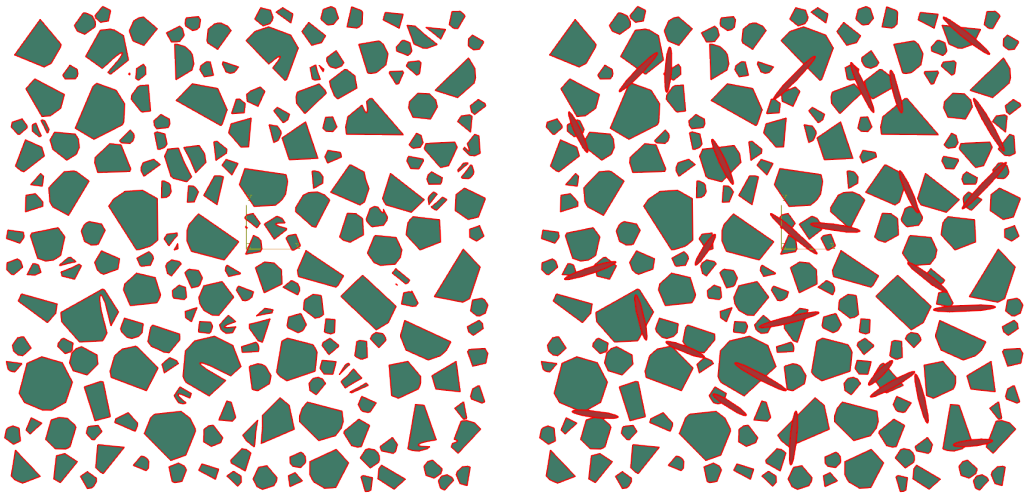

Figure B.2: Aggregates Part with the removed and then added crack section

Following the same procedure for the mortar part by defining the part, removing the Aggregate-Crack combination section and then merging them together results in the final part that can be used as the concrete model.

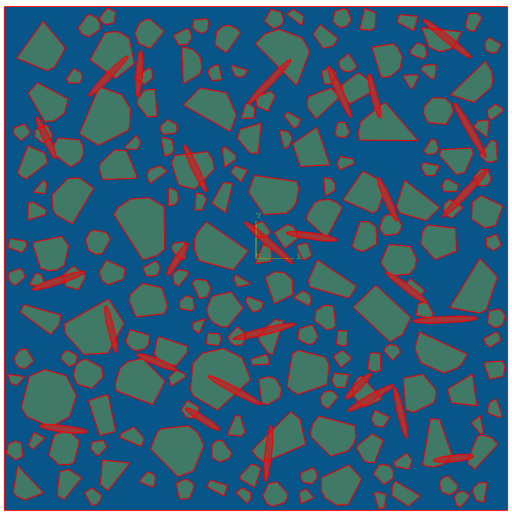

Figure B.3: The concrete model in ABAQUS consist of aggregate, crack and mortar parts merged together

References

[1] J. Moon, S. Speziale, C. Meral, B. Kalkan, S. M. Clark, and P. J. Monteiro, "Determination of the elastic properties of amorphous materials: Case study of alkali–silica reaction gel," *Cement and Concrete Research*, vol. 54, pp. 55 – 60, 2013.

[2] T. Naik, V. Malhotra, and J. Popovics, *The ultrasonic pulse velocity method*, pp. 8–1–8–19. CRC Press, 1 2003.

[3] J. Zhu and J. S. Popovics, "Imaging concrete structures using air-coupled impact-echo," *Journal of Engineering Mechanics*, vol. 133, no. 6, pp. 628–640, 2007.

[4] P. Anugonda, J. S. Wiehn, and J. A. Turner, "Diffusion of ultrasound in concrete," *Ultrasonics*, vol. 39, no. 6, pp. 429 – 435, 2001.

[5] S. K. Ramamoorthy, Y. Kane, and J. A. Turner, "Ultrasound diffusion for crack depth determination in concrete," *The Journal of the Acoustical Society of America*, vol. 115, no. 2, pp. 523–529, 2004.

[6] F. Deroo, "Damage detection in concrete using diffuse ultrasound measurements and an effective medium theory," Master's thesis, Georgia Institute of Technology, Dec. 2009.

[7] F. Deroo, J.-Y. Kim, J. Qu, K. Sabra, and L. J. Jacobs, "Detection of damage in concrete using diffuse ultrasound," *The Journal of the Acoustical Society of America*, vol. 127, no. 6, pp. 3315–3318, 2010.

[8] R. Snieder, A. Grêt, H. Douma, and J. Scales, "Coda wave interferometry for estimating nonlinear behavior in seismic velocity," *Science*, vol. 295, no. 5563, pp. 2253–2255, 2002.

[9] O. I. Lobkis and R. L. Weaver, "Coda-wave interferometry in finite solids: Recovery of p-to-s conversion rates in an elastodynamic billiard," *Phys. Rev. Lett.*, vol. 90, p. 254302, Jun 2003.

[10] E. Larose and S. Hall, "Monitoring stress related velocity variation in concrete with a 2105 relative resolution using diffuse ultrasound," *The Journal of the Acoustical Society of America*, vol. 125, no. 4, pp. 1853–1856, 2009.

[11] D. P. Schurr, J.-Y. Kim, K. G. Sabra, and L. J. Jacobs, "Damage detection in concrete using coda wave interferometry," *NDT E International*, vol. 44, no. 8, pp. 728 – 735, 2011.

[12] A. Asadollahi and L. Khazanovich, "Numerical investigation of the effect of heterogeneity on the attenuation of shear waves in concrete," *Ultrasonics*, vol. 91, pp. 34 – 44, 2019.

[13] L. Sanchez, B. Fournier, M. Jolin, and J. Duchesne, "Reliable quantification of aar damage through assessment of the damage rating index (DRI)," *Cement and Concrete Research*, vol. 67, pp. 74 – 92, 2015.

[14] L. Sanchez, B. Fournier, M. Jolin, M. A. B. Bedoya, J. Bastien, and J. Duchesne, "Use of damage rating index to quantify alkali-silica reaction damage in concrete: Fine versus coarse aggregate," *ACI Materials Journal*, vol. 113, 01 2016.

[15] B. P. Gautam and D. K. Panesar, "The effect of elevated conditioning temperature on the asr expansion, cracking and properties of reactive spratt aggregate concrete," *Construction and Building Materials*, vol. 140, pp. 310 – 320, 2017.

[16] L. J. Struble and S. Diamond, "Swelling properties of synthetic alkali silica gels," *Journal of the American Ceramic Society*, vol. 64, no. 11, pp. 652–655, 1981.

[17] Z. Tian, L. Huo, W. Gao, H. Li, and G. Song, "Modeling of the attenuation of stress waves in concrete based on the rayleigh damping model using time-reversal and PZT transducers," *Smart Materials and Structures*, vol. 26, p. 105030, sep 2017.

[18] M. Gresil and V. Giurgiutiu, "Prediction of attenuated guided waves propagation in carbon fiber composites using rayleigh damping model," *Journal of Intelligent Material Systems and Structures*, vol. 26, no. 16, pp. 2151–2169, 2015.

[19] A. Zerwer, G. Cascante, and J. Hutchinson, "Parameter estimation in finite element simulations of rayleigh waves," *Journal of Geotechnical and Geoenvironmental Engineering*, vol. 128, no. 3, pp. 250–261, 2002.

[20] F. Moser, L. J. Jacobs, and J. Qu, "Modeling elastic wave propagation in waveguides with the finite element method," *NDT E International*, vol. 32, no. 4, pp. 225 – 234, 1999.

[21] M. B. Drozdz, *Efficient finite element modelling of ultrasound waves in elastic media*. PhD thesis, Imperial College London (University of London), Jan. 2008.

[22] D. Alleyne and P. Cawley, "A two-dimensional fourier transform method for the measurement of propagating multimode signals," *The Journal of the Acoustical Society of America*, vol. 89, no. 3, pp. 1159–1168, 1991.

[23] J. Zhu, J. S. Popovics, and F. Schubert, "Leaky rayleigh and scholte waves at the fluid–solid interface subjected to transient point loading," *The Journal of the Acoustical Society of America*, vol. 116, no. 4, pp. 2101–2110, 2004.

[24] T. Planès and E. Larose, "A review of ultrasonic coda wave interferometry in concrete," *Cement and Concrete Research*, vol. 53, pp. 248 – 255, 2013.

[25] R. Snieder, "The theory of coda wave interferometry," *Pure and Applied Geophysics*, vol. 163, pp. 455–473, Mar 2006.

[26] P. Roberts, "Development of the active doublet method for monitoring small changes in crustal properties," *Seismol Res Lett*, vol. 62, no. 1, pp. 36–37, 1991. cited By 1.

[27] G. Chen, D. Pageot, J.-B. Legland, O. Abraham, M. Chekroun, and V. Tournat, "Numerical modeling of ultrasonic coda wave interferometry in a multiple scattering medium with a localized nonlinear defect," *Wave Motion*, vol. 72, pp. 228 – 243, 2017.

[28] F. Deroo, L. J. Jacobs, J. Kim, J. Qu, and K. Sabra, "Damage detection in concrete using diffuse ultrasound measurements," *AIP Conference Proceedings*, vol. 1211, no. 1, pp. 1509–1516, 2010.